

The Texas Medical Center Library

DigitalCommons@TMC

The University of Texas MD Anderson Cancer
Center UTHealth Graduate School of
Biomedical Sciences Dissertations and Theses
(Open Access)


The University of Texas MD Anderson Cancer
Center UTHealth Graduate School of
Biomedical Sciences

8-2019

Modeling Proton Relative Biological Effectiveness Using Monte Carlo Simulations of Microdosimetry

Mark A. Newpower

Follow this and additional works at: https://digitalcommons.library.tmc.edu/utgsbs_dissertations

 Part of the [Biological and Chemical Physics Commons](#), [Oncology Commons](#), [Other Medical Sciences Commons](#), [Other Physical Sciences Commons](#), and [the Radiation Medicine Commons](#)

Recommended Citation

Newpower, Mark A., "Modeling Proton Relative Biological Effectiveness Using Monte Carlo Simulations of Microdosimetry" (2019). *The University of Texas MD Anderson Cancer Center UTHealth Graduate School of Biomedical Sciences Dissertations and Theses (Open Access)*. 950.
https://digitalcommons.library.tmc.edu/utgsbs_dissertations/950

This Dissertation (PhD) is brought to you for free and open access by the The University of Texas MD Anderson Cancer Center UTHealth Graduate School of Biomedical Sciences at DigitalCommons@TMC. It has been accepted for inclusion in The University of Texas MD Anderson Cancer Center UTHealth Graduate School of Biomedical Sciences Dissertations and Theses (Open Access) by an authorized administrator of DigitalCommons@TMC. For more information, please contact digitalcommons@library.tmc.edu.


The
TMC LIBRARY
Health Sciences Resource Center

MODELING PROTON RELATIVE BIOLOGICAL EFFECTIVENESS USING MONTE
CARLO SIMULATIONS OF MICRODOSIMETRY


by


Mark Andrew Newpower, M.S., B.S.

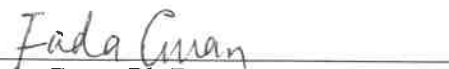
APPROVED:



Radhe Mohan, Ph.D.
Advisory Professor


Uwe Titt, Ph.D.


Narayan Sahoo, Ph.D.


Oleg Vassiliev, Ph.D.


Fada Guan, Ph.D.


David Grosshans, M.D., Ph.D.


Suyu Liu, Ph.D.

APPROVED:

Dean, The University of Texas
MD Anderson Cancer Center UTHHealth Graduate School of Biomedical Sciences

MODELING PROTON RELATIVE BIOLOGICAL EFFECTIVENESS USING MONTE
CARLO SIMULATIONS OF MICRODOSIMETRY

A

DISSERTATION

Presented to the Faculty of

The University of Texas

MD Anderson Cancer Center UTHealth

Graduate School of Biomedical Sciences

in Partial Fulfillment

of the Requirements

for the Degree of

DOCTOR OF PHILOSOPHY

by

Mark Andrew Newpower, M.S., B.S.
Houston, Texas

August, 2019

Acknowledgements

The journey through graduate school to earn a PhD is a long one and is filled with countless people who help along the way.

I would like to thank my advisor, Dr. Radhe Mohan for taking me on as a graduate student and mentoring me these past four years. It has been an honor to work with you and to develop my skills as a scientist under your tutelage. I am forever grateful for your time and your advice over the years.

My advisory committee also deserves thanks. Dr. Uwe Titt, Dr. Oleg Vassiliev, Dr. Fada Guan, Dr. Narayan Sahoo, Dr. David Grosshans and Dr. Suyu Liu all helped guide my work and gave me valuable advice about my project. Dr. Titt and I met almost weekly and published a paper together on a side project we had. I am thankful for his mentoring and for teaching me more about Monte Carlo, publishing papers, and obscure German words. Dr. Vassiliev had the idea to use Geant4 DNA to create a virtual “measurement” of microdosimetry, and he had a great hand in the beginning of this project. Dr. Guan gave me essential advice on Monte Carlo simulation and on his RBE experiments, two of which I use in this work. Dr. Sahoo gave me excellent feedback on the clinical impact of my project, and I am thankful for the advice from such a figure in the proton therapy world. Dr. Grosshans gave me his perspective on what a radiation oncologist is looking for in treatment plans and what a variable RBE means to clinicians. He also helped guide the treatment planning in this work. Finally, Dr. Liu acted as a great outside member of my committee, and forced me to present my work in a way that is more understandable. Her feedback on microdosimetry distributions changed the course of my project.

I also received significant support from outside of MD Anderson. Dr. Pankaj Chaudhary, Dr. Stephen McMahon and Dr. Kevin Prise from Queen's University Belfast, Northern Ireland, and Dr. Giuseppe Schettino from National Physical Laboratory, UK, contributed to this project and are coauthors on the paper I published based on this work. They injected fresh ideas into the project and brought my manuscript up to a standard I couldn't achieve alone. I also want to thank Hans-Peter Wieser at the German Cancer Research Center, DKFZ in Heidelberg, Germany for helping me understand the inner workings of matRad.

The members of the Medical Physics program also deserve praise. Thank you to Betsy Kindred, Frances Quintana and Anne Baronitis for running the program and making student life easier. I also want to thank Dr. Richard Wendt and Dr. Rebecca Howell, the program directors who admitted me and gave me a chance to come to MD Anderson and join such an outstanding program.

I would like to thank my parents, Scott and Mary, as well as my brother Thomas. My dad taught me how to work tirelessly to master a subject, a skill invaluable in research. My mom taught me to give my full passion and commitment every day, and to always do the right thing. Tommy has helped me move across the country a couple of times and is only a phone call away for support. I hope I have made each of you proud.

Last but certainly not least, I would like to thank my wife Mereta. You have celebrated with me during the highs and cheered me up from the lows of graduate school. You also took on most of the childcare duties, and stepped up when I had to travel for conferences and interview. I have an amazing home life because of your love and sacrifice. I could not have done this without you. You make me a better person and I love you.

MODELING PROTON RELATIVE BIOLOGICAL EFFECTIVENESS USING MONTE CARLO SIMULATIONS OF MICRODOSIMETRY

Mark Andrew Newpower, M.S., B.S.

Advisory Professor: Radhe Mohan, Ph.D.

Proton therapy is a radiotherapy modality that can offer a better physical dose distribution when compared to photon radiotherapy by taking advantage of the Bragg peak, a narrow region of rapid energy loss. Proton therapy is also known to offer an enhanced relative biological effectiveness (RBE) compared to photons. In the current clinical standard, RBE is fixed at 1.1 at all points along the proton beam, meaning protons are assumed to require 10% less dose than photons to achieve target coverage and organ at risk (OAR) sparing. However, there is mounting clinical evidence, and a significant number of in vitro experiments, that show RBE varies, typically as a function of dose averaged linear energy transfer (LET_D).

There are two goals of this work. The first is to develop a novel method to model proton RBE by using the microdosimetric kinetic model (MKM). The MKM requires a quantity called dose mean lineal energy ($\overline{y_D}$), which is analogous to LET_D , to model RBE. In this work, a novel method to calculate $\overline{y_D}$ is proposed, based on the proton energy spectrum at a location, and Monte Carlo simulations of microdosimetry. The second goal of this work is to implement MKM into a treatment planning system to assess the theoretical clinical impact of including variable RBE during treatment plan optimization.

This work presents a method to calculate $\overline{y_D}$ and model the RBE of several proton RBE experiments. The variable RBE of these experiments was modeled more accurately by MKM than previously proposed phenomenological models. However, a clear superiority over an LET_D-based model was not demonstrated. In a treatment planning exercise, including variable RBE modeling into the optimization algorithm led to increased target coverage while maintaining the dose sparing of OARs. Based on the parameters chosen for the MKM, this led to an increase in physical dose delivered to the brainstem, and when reanalyzed assuming an RBE = 1.1, led to doses beyond tolerance. In conclusion, this work presents a novel method to compute $\overline{y_D}$ for input into the MK model, and demonstrates slight potential benefits of considering a variable RBE in treatment plan optimization.

Table of Contents

Approval Page.....	i
Title Page	ii
Acknowledgements	iii
Abstract	v
Abbreviations	xiii
Chapter 1: Introduction	1
1.1 Proton therapy	1
1.2 Relative biological effectiveness.....	2
1.3 Scope of Dissertation and Specific Aims	4
Chapter 2: Methods and Materials	7
2.1 RBE Data.....	7
2.2 RBE models.....	8
2.3 Calculating $\overline{y_D}$ and fitting MKM to experimental data.....	13
2.3.1 Computational Resources	13
2.3.2 Geant4 DNA	14
2.3.3 Calculating y and $f(y)$	15
2.3.4 Calculating $\overline{y_D}$ of a polyenergetic proton beam	16
2.4 Fitting r_d and calculating RBE.....	17
2.5 Comparing RBE models.....	18

2.6 matRad	19
2.6.2 Patient data	25
2.6.3 Radiobiological properties of tissues during MKM optimization.....	26
2.6.4 Comparing standard treatment plans to MKM optimized plans.....	28
Chapter 3: Results	30
3.1 Phenomenological model fitting to experimental RBE data.....	30
3.2 Difference between phenomenological RBE models and RBE data	32
3.3 Fractional error of Geant4 DNA $f(y)$ scoring method.....	36
3.4 Calculating $\overline{y_D}$	38
3.5 Modeling RBE with the generic RBE model and the MK model.....	41
3.6 AIC analysis of generic RBE model vs. the MK model	43
3.7 matRad Optimization Results	45
Chapter 4: Discussion	58
4.1 Difference between phenomenological models and experimental RBE data	58
4.2 Fitting the generic RBE model to data.....	60
4.3 Uncertainty analysis of Geant4 DNA $f(y)$ scoring method.....	60
4.4 Calculating $\overline{y_D}$	61
4.5 MKM fitting of experimental RBE data	62
4.6 AIC analysis of generic RBE model vs. MK model	63
4.7 MKM Optimization in matRad	64
Chapter 5: Conclusion.....	71

5.1 Difference between phenomenological models and experimental RBE data	71
5.2 Comparing the MK model to a generic LET _D based RBE model.....	71
5.3 Creating biologically-optimized treatment plans with matRad.....	72
5.4 Future directions.....	72
Chapter 6: References	74
Vita.....	84

List of Figures

Figure 1: Comparison of proton and photon depth-dose curves.....	2
Figure 2: matRad GUI	20
Figure 3: yD_table_MDA_G3.mat format	23
Figure 4: RBE optimization implemented into matRad.	25
Figure 5: Phenomenological and generic RBE models applied to the Chaudhary et al and Guan and Bronk et al data.	31
Figure 6: Models applied to RBE data from Patel and Bronk et al	32
Figure 7: Fractional Error, samples per track, and number of tracks sampled using Geant4 DNA	37
Figure 8: $\overline{y_D}$ values for monoenergetic proton beams	39
Figure 9: Relationship between $\overline{y_D}$ and LET _D	40
Figure 10: Generic RBE model and MK model applied to Guan and Bronk et al data.....	41
Figure 11: Generic RBE model and MK model applied to Chaudhary et al data.	42
Figure 12: Generic RBE model and MK model applied to Patel and Bronk et al data.	43
Figure 13: IDD _s and $\overline{y_D}$ as a function of depth for two beams.....	47
Figure 14: Dose volume histograms of the RBE-weighted doses of the std_opt and std_opt_MKM_calc plan.	48
Figure 15: RBE in the brainstem, GTV and CTV as calculated by the MKM.....	49
Figure 16: Comparison of std_opt to std_opt_MKM_calc	50
Figure 17: MKM optimization plan reduces RWD brainstem hotspot.....	51
Figure 18: DVH comparison of std_opt_MKM_calc and MKM_opt	53
Figure 19: $\overline{y_D}$ distribution before and after MKM optimization.....	54
Figure 20: Difference in physical dose distributions between std_opt and MKM_opt plan	55

Figure 21: RWD for MKM_opt plan and MKM_opt plan recalculated with $RBE = 1.1$ 57

List of Tables

Table 1: α_x and β_x parameters for RBE data.	8
Table 2: Organ at risk constraints for ependymoma patients.	26
Table 3: Radiobiological properties of tissues for RBE optimization	27
Table 4: Guan and Bronk et al H460 data compared to phenomenological RBE models.....	33
Table 5: Guan and Bronk et al H1437 data compared to phenomenological RBE models.....	33
Table 6: Chaudhary et al pristine Bragg peak data compared to phenomenological RBE models.	34
Table 7: Chaudhary et al SOBP peak data compared to phenomenological RBE models.	35
Table 8: Patel and Bronk et al H460 data compared to phenomenological RBE models.	35
Table 9: AIC analysis of generic RBE model vs MK model.....	44
Table 10: Dose to targets and OARs for IMPT plans	46
Table 11: DVH metrics for MKM optimized plan analyzed with variable RBE and RBE=1.1..	56

Abbreviations

CI	Confidence Interval
CTV	Clinical target volume
DVH	Dose volume histogram
EUD	Equivalent uniform dose
GTV	Gross tumor volume
IDD	Integrated depth dose
IMPT	Intensity modulated proton therapy
LET _D	Dose averaged linear energy transfer
MKM	Microdosimetric kinetic model
NTCP	Normal tissue complication probability
RBE	Relative biological effectiveness
r_d	Radius of the domain
RL	Relative likelihood
RWD	RBE-weighted dose
SOBP	Spread out Bragg peak
SS	Sum of squares
TD ₅₀	Dose at which a particular complication is expected in 50% of a given population
TPS	Treatment planning system
$\overline{y_D}$	Dose mean lineal energy

Chapter 1: Introduction

1.1 Proton therapy

Proton therapy is a radiotherapy treatment modality whereby protons are accelerated to high energies and then used to irradiate a tumor. Robert Wilson, a physicist at Harvard University, first proposed proton therapy in 1946 [1]. Wilson proposed that protons be used for therapy due their unique physical characteristic, the Bragg peak. As protons are transported through a medium, they gradually lose energy. This energy loss is quantified by stopping power S . After the proton has lost most of its initial kinetic energy, stopping power rapidly increases with continued energy loss, until all kinetic energy is lost. The rapid increase in stopping power results in the Bragg peak, a narrow region with large amounts of energy deposited. Wilson proposed that several proton energies be used to create a spread-out Bragg peak (SOBP), which can provide adequate dose distribution across a target volume. A schematic comparing single Bragg peaks, a spread out Bragg peak and the depth-dose curve for an MV photon beam is shown in Fig. 1. When comparing the depth-dose curve of protons to photons the physical advantage of protons becomes clear. Photon beams are characterized by having a dose peak at relatively shallow depths with a long “tail” that extends beyond the depth of the patient. The physical nature of photons means there is significant dose to tissue upstream and downstream from the target. Contrast this to a proton SOBP, which results in rapid dose fall off over a few millimeters at the beam’s distal edge. Theoretically this means that a critical structure such as the heart, spinal cord or brain stem could be placed in close proximity to the SOBP.

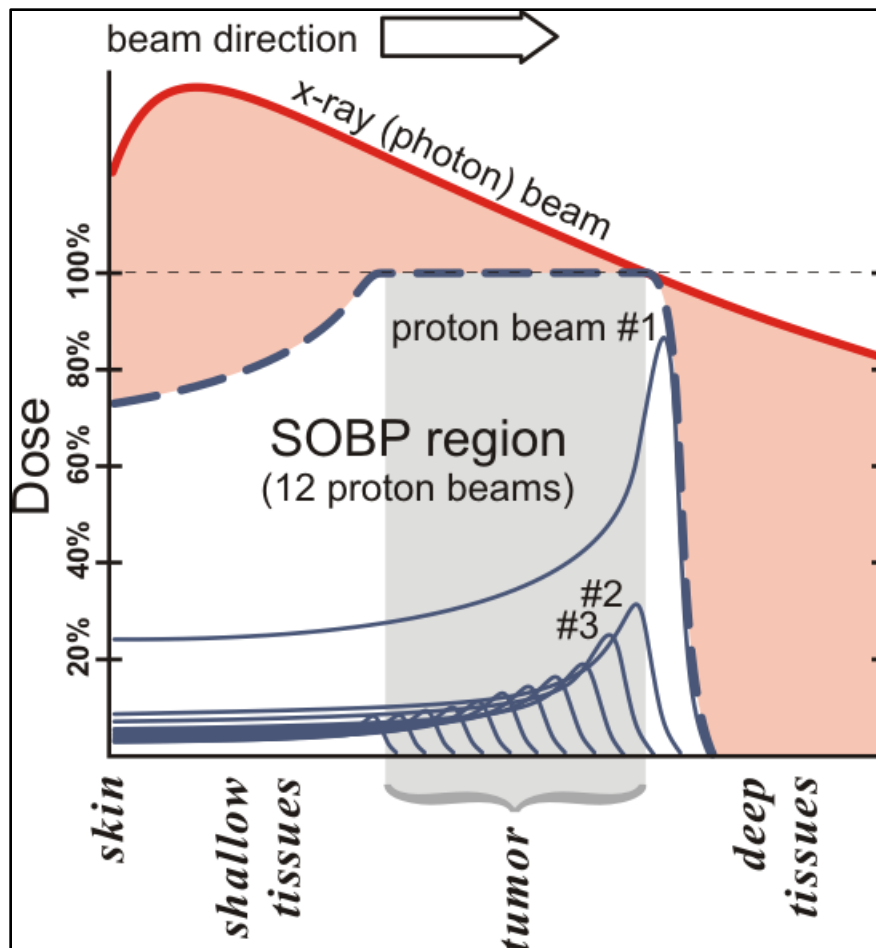


Figure 1: Comparison of proton and photon depth-dose curves.

Multiple pristine Bragg peaks (blue solid lines) are irradiated onto a target to achieve a spread out Bragg peak (blue dashed line). The various heights of the pristine beams indicate each beam is given a different weight to ensure a flat SOBP. This image “Comparison_of_dose_profiles_for_proton_v._x-ray_radiotherapy.png” by MarkFilipak is licensed under CC BY-SA 3.0 (https://en.wikipedia.org/wiki/File:Comparison_of_dose_profiles_for_proton_v._x-ray_radiotherapy.png).

1.2 Relative biological effectiveness

There is also a radiobiological rationale for using proton therapy: protons have an increased biological effectiveness compared to photons. This is quantified with relative biological effectiveness (RBE), defined as the ratio of doses for two different radiation types to

reach the same biological endpoint. Convention dictates that the reference radiation dose goes in the numerator, and the proton dose in the denominator, resulting in an RBE value greater than 1.

$$RBE = \frac{D_{ref}}{D_{proton}} \quad (1)$$

Currently in clinical practice, proton RBE is assumed to be 1.1 at all points along the Bragg curve. However Paganetti showed, according to most cell survival experiments, RBE values for proton therapy vary along the Bragg curve. RBE in the entrance region is ~ 1.1 , rising to ~ 1.15 in the Bragg peak and SOBP, and increasing to ~ 1.35 in the distal edge and ~ 1.7 in the distal falloff region [2]. While wide variations in RBE are observed, Paganetti concluded that on average, for most of the Bragg curve, the RBE has a value of ~ 1.1 . RBE is typically modeled as a function of dose-averaged linear energy transfer (LET_D), a physical quantity that is straightforward to calculate with Monte Carlo simulations such as GATE [3, 4], FLUKA [5], GEANT4 [6] or TOPAS [7] or analytical functions [8, 9]. Clinical proton beams typically have LET_D values that reach a maximum around 20-25 keV/ μ m. In this range, most data show a linear relationship of RBE as a function of LET_D [10]. As summarized by Grün et al, most $RBE(LET_D)$ experiments have been measured in regions where the LET distribution is relatively narrow [11]. However, as noted by Grün et al and Mohan et al, in regions such as an SOBP or overlapping fields, the LET distribution may be broad and the $RBE(LET_D)$ relationship is no longer linear [11, 12].

Clinical evidence of variable proton RBE is scarce but concerning. Peeler et al analyzed a set of pediatric ependymoma patients who had T2-FLAIR hyperintensity regions in MR images after proton therapy and showed that these regions are highly correlated with increased LET, and therefore increased RBE [13]. A paper published after the National Cancer Institute (NCI) hosted a workshop on radiobiological issues in charged particle therapy noted that as the

number of patients treated with proton therapy increases, so do the reports of unexpected toxicities [14]. In another NCI workshop, brainstem injuries in pediatric patients undergoing proton therapy were discussed and recommendations were made for modifying treatment plans in order to reduce these injuries [15]. Underwood et al showed in a cohort of lung cancer patients receiving proton therapy that RBE exceeded 1.1 based on follow up CT scans that showed increased lung tissue density [16]. These examples should make it clear that the topic of proton biological effectiveness should be further studied, and eventually should be taken into account when creating the proton treatment plans of the future.

1.3 Scope of Dissertation and Specific Aims

In current clinical practice, the relative biological effectiveness (RBE) of proton beams is assumed to be 1.1 at all points along the Bragg curve. However, several recent experiments have shown that the RBE of therapeutic proton beams can be as high as 2 or greater in the region distal to the Bragg peak [17-19]. This RBE is significantly different than the standard clinical practice of using a constant RBE of 1.1, meaning the tissue in the region distal to the Bragg peak is receiving significantly more damage. At present, there has been limited work showing that the microdosimetric kinetic model (MKM) can be used to predict such high RBEs in proton therapy.

Accurate prediction of the RBE at each point along the Bragg curve would enable biologically-optimized treatment plans, which have the potential to offer improved treatments for proton therapy patients. By quantifying the RBE at all points along the proton beam, clinical physicists will be able to place the most damaging parts of the beam within the target and take full advantage of proton therapy's biological dose distribution. MKM is a first-principle model that predicts cell survival based on dose deposition on a scale of micrometers, and has been used to model carbon ion RBE, but has not yet been applied clinically to proton therapy. The central

goal of this project is to determine how well MKM can accurately predict RBE in the high LET region of the proton beam and to develop a treatment planning system that implements MKM to predict proton RBE. The following Specific Aims will address this central goal:

Aim One: *Evaluate the accuracy of phenomenological RBE models in the Bragg peak and distal falloff region.* Several RBE models have already been proposed, which typically model RBE as a linear function of LET. However, recent RBE data shows strong evidence that RBE may in fact be a nonlinear function of LET, especially beyond the Bragg peak. The hypothesis for this Aim is: in the high linear energy transfer (LET) region at and beyond the Bragg peak, phenomenological RBE models will underestimate RBE by at least 20%. This Aim will determine the applicability of phenomenological RBE models in the high LET region and possibly demonstrate the need for a model that accurately predicts the high RBEs in these regions.

Aim Two: *Optimize the microdosimetric parameters to achieve a best fit for observed RBE data based on the MKM.* I propose a method to calculate microdosimetric quantities that uses the proton energy spectrum at various locations along the Bragg curve, based on calculations using the Geant4 DNA toolkit. The method will be tested with three data sets, consisting of seven total experiments across three different proton beamlines. I hypothesize this MK model will predict the RBEs at all points along the proton beam, including the Bragg peak and distal falloff regions, within experimental uncertainties. This Aim will also obtain the optimal parameters for fitting MKM to experimental data, demonstrating the best fit achievable using MKM.

Aim Three: *Develop a variable RBE prediction functionality in a treatment planning system for proton therapy.* The goal of this Aim is to implement the MKM into matRad, an open-source treatment planning system that allows the user to access all radiation calculations and even add

their own functionalities to the software. Successful completion of this Aim would enable a treatment planning system to biologically optimize a proton therapy treatment plan, a feature needed clinically, but not yet developed. Treatment plans optimized using a variable RBE will be compared to those optimized with a constant 1.1 RBE to investigate whether variable RBE plans can improve the therapeutic ratio.

The work described above will develop a method for using experimental biological data and microdosimetry to predict RBE in a treatment planning system for proton therapy. In current proton therapy treatment, variable RBE is not considered, likely resulting in an overdosing of tissues at and distal to the Bragg peak. This project is innovative in that it seeks to bring variable RBE prediction into clinical use, a capability that has not been realized, and has the potential to lead to better patient outcomes by placing the most biologically damaging regions of the proton beam into the target volumes.

Chapter 2: Methods and Materials

This chapter is based upon a paper reprinted from International Journal of Radiation Oncology*Biology*Physics, Vol. 104, Issue 2, Mark Newpower, Darshana Patel, Lawrence Bronk, Fada Guan, Pankaj Chaudhary, Stephen J. McMahon, Kevin M. Prise, Giuseppe Schettino, David R. Grosshans, Radhe Mohan, Using the Proton Energy Spectrum and Microdosimetry to Model Proton Relative Biological Effectiveness, Pages 316-324 Copyright 2019 with Permission from Elsevier. 2019,ISSN 0360-3016, <https://doi.org/10.1016/j.ijrobp.2019.01.094>.

(<http://www.sciencedirect.com/science/article/pii/S0360301619301853>)

2.1 RBE Data

The RBE data used in this work have been previously published by Chaudhary et al, Guan and Bronk et al and Patel and Bronk et al [17-19]. In each of these three data sets the authors performed cell survival experiments and fit the clonogenic cell survival data for protons and photon beams with the linear quadratic (LQ) model. These model parameters were then used to calculate RBE at various cell survival levels (i.e. 10%, 50%, etc.). These experiments were performed on three different beamlines: at the Proton Therapy Center Houston (PTCH) at MD Anderson Cancer Center [18], at Centro di AdroTerapia Applicazioni Nucleari Avanzate (CATANA) in Catania, Italy [17], and at the Heidelberg Ion Therapy Center (HIT) in Heidelberg, Germany [19]. For each experiment the LET_D was calculated at each RBE measurement point to enable modeling RBE as a function of LET_D. The experiments by Guan and Bronk et al and Patel and Bronk et al were done only along a pristine Bragg peak, while Chaudhary et al used both a pristine Bragg peak and an SOBP for their experiments. Four cell

lines were utilized in these studies: AGO1522 and U87 (Chaudhary et al), H460 and H1437 (Guan and Bronk et al), while Patel and Bronk et al performed a very similar RBE experiment to Guan and Bronk et al, with only H460 cells. The α_x and β_x values for each study are presented in Table 1. For all RBE calculations in this work, RBE was calculated at the 10% clonogenic survival level.

Table 1: α_x and β_x parameters for RBE data.

The α_x and β_x parameters shown here were taken from the RBE studies. These values are used as input in RBE model calculations.

Cell line	α_x [Gy ⁻¹]	β_x [Gy ⁻²]
Guan and Bronk et al [18]		
H460	0.290	0.083
H1437	0.05	0.041
Patel and Bronk et al [19]		
H460	0.290	0.083
Chaudhary et al [17]		
AGO1522	0.54	0.062
U87	0.110	0.06

2.2 RBE models

Despite Paganetti's conclusion that RBE should remain fixed at 1.1 for now, there is mounting clinical evidence that assuming an RBE = 1.1 in treatment planning leads to image changes along the proton beam's distal edge. Peeler et al. showed these MR image changes are well correlated with high LET regions in children treated for ependymoma [13]. Underwood et al. demonstrated the distal edge region of the proton beam corresponds to increased Hounsfield Unit changes in CT scans of lung patients following radiation therapy, and linked these changes to an RBE > 1.1 [16]. Therefore there is a clinical interest in understanding how RBE varies along the path of the proton beam. If clinical physicists were able to model a variable RBE in the treatment planning system, then treatment plans could be optimized to deliver high RBE

radiation to the target tissue and spare normal tissue with low RBE radiation. Several phenomenological RBE models have been proposed [20] and three are summarized below.

The model proposed by Wedenberg et al [21] assumes a constant value for β , while α is linearly dependent on LET_D , a fitting parameter q and the x-ray α/β ratio $(\alpha/\beta)_x$:

$$\alpha = \alpha_x \left(1 + \frac{qLET_d}{(\alpha/\beta)_x} \right) \quad (2)$$

The value for q was found by fitting across 10 cell lines and has a value of 0.434 Gy $\mu\text{m}/\text{keV}$.

The value for q is assumed to be the same regardless of cell type or the physical characteristic of the proton beam. Wedenberg et al caution, however, that this equation is not valid for LET_D higher than 30 keV/ μm .

The RBE model proposed by Carabe-Fernandez et al takes into account RBE's dependence on LET in the RBE_{min} and RBE_{max} terms and is also based on the LQ model [22, 23]. The coefficients in the model's RBE_{min} and RBE_{max} terms were determined via linear regression of previously published RBE experiments. This RBE model also requires as input the physical proton dose, which will be set to 1.8 Gy throughout this work.

$$\begin{aligned} & RBE \left[D_p, \left(\frac{\alpha}{\beta} \right)_x, LET_D \right] \\ &= \frac{1}{2D_p} \left(\sqrt{\left(\frac{\alpha}{\beta} \right)_x^2 + 4D_p \left(\frac{\alpha}{\beta} \right)_x RBE_{max} + 4D_p^2 RBE_{min}^2} - \left(\frac{\alpha}{\beta} \right)_x \right) \end{aligned} \quad (3)$$

$$RBE_{max} = 0.843 + 1.54 \frac{2.686}{\left(\frac{\alpha}{\beta}\right)_x} LET_D \quad (4)$$

$$RBE_{min} = 1.09 + 0.006 \frac{2.686}{\left(\frac{\alpha}{\beta}\right)_x} LET_D \quad (5)$$

McNamara, Schuemann and Paganetti [24] developed an RBE model based on the concepts of RBE_{min} and RBE_{max} proposed by Carabe et al [22] as well as on a dependence on $\sqrt{(\alpha/\beta)_x}$ proposed by Jones [25]. Like the Carabe-Fernandez model, this model requires the physical proton dose as input, and is set to 1.8 Gy throughout this work. The McNamara et al model has the form:

$$RBE \left[D_p, \left(\frac{\alpha}{\beta} \right)_x, LET_D \right] \quad (6)$$

$$= \frac{1}{2D_p} \left(\sqrt{\left(\frac{\alpha}{\beta} \right)_x^2 + 4D_p \left(\frac{\alpha}{\beta} \right)_x \left(p_0 + \frac{p_1}{\left(\frac{\alpha}{\beta} \right)_x} LET_D \right) + 4D_p^2 \left(p_2 + p_3 \sqrt{\left(\frac{\alpha}{\beta} \right)_x} LET_D \right)} - \left(\frac{\alpha}{\beta} \right)_x \right)$$

The fitting coefficients $p_0 - p_3$ were found to be: $p_0 = 0.999064$ (standard error) (SE) 0.014125, $p_1 = 0.35605$ (SE 0.015038), $p_2 = 1.1012$ (SE 0.0059972), and $p_3 = -0.0038703$ (SE 0.00091303), with a R^2 value of 0.255. The McNamara model was shown to predict RBE values well at low LET_D . However at higher LET_D values (~ 18.7 keV/ μ m), the model predicts a lower RBE than measured experimentally by Guan and Bronk et al.

To facilitate comparison to the microdosimetric kinetic model (MKM) a generic LET_D based model with a single fitting parameter was proposed:

$$\alpha_p = \alpha_x + k \times LET_D \quad (7)$$

This model assumes β is constant for both proton and X-ray beams. The k parameter was varied to achieve a best fit with the experimental RBE data. This generic RBE model enabled a comparison to the MKM because both models have one free fitting parameter. The method to compare the MKM and generic RBE model is outlined in section 2.5.

A first-principle approach to predicting cell survival known as the microdosimetric kinetic model (MKM) was proposed by Hawkins [26, 27]. His work built upon the theory of dual radiation action, developed by Kellerer and Rossi, and Zaider and Rossi [28, 29]. As its name implies, MKM uses the concepts of microdosimetry, the study and quantification of spatial and temporal distributions of absorbed energy in irradiated matter [30, 31]. The central concept of microdosimetry is the domain, a spherical volume of unit density. The radius of the domain (r_d) is typically on the order of 0.5 μm . The domain is defined as the distance a DNA lesion can travel through the nucleus before it is repaired [27]. Thus, the domain is a cell-specific parameter that depends on the cell's ability to repair damage to its DNA. If the domain is placed randomly near an ion track, there is a probability that energy will be deposited inside it. The simplest microdosimetric quantity is specific energy z , which has units of J/kg, or Gray, and can be considered as a stochastic equivalent of absorbed dose [30]. Specific energy can be averaged in two ways: frequency-averaged and dose-averaged, $\overline{z_F}$ and $\overline{z_D}$, respectively. Another quantity of interest is lineal energy y , which is defined as the quotient of the energy deposited

into the domain ε by a primary particle, with mean chord length \bar{l} through that volume, expressed in Eq. 8.

$$y = \frac{\varepsilon}{\bar{l}} \quad (8)$$

Lineal energy has units of keV/ μm . In the same way as specific energy, the lineal energy frequency distribution function can be used to calculate frequency averaged ($\overline{y_F}$) and dose averaged ($\overline{y_D}$) lineal energy. The single event distributions of specific energy ($f(z)$) and lineal energy ($f(y)$) are used to compute frequency and dose averaged specific and lineal energy in the following way:

$$\overline{z_F} = \int_0^\infty z f(z) dz \quad (9)$$

$$\overline{y_F} = \int_0^\infty y f(y) dy \quad (10)$$

$$\overline{z_D} = \frac{\int_0^\infty z^2 f(z) dz}{\overline{z_F}} \quad (11)$$

$$\overline{y_D} = \frac{\int_0^\infty y^2 f(y) dy}{\overline{y_F}} \quad (12)$$

The quantity $\overline{y_D}$ is particularly important in the MK model when used to model ion irradiation survival experiments. It is the stochastic quantity in microdosimetry that corresponds to LET_D . Both LET_D and $\overline{y_D}$ are used as measures of radiation quality and as a surrogate for biological response. For proton therapy studies this work used the MKM equations presented by Kase et al [32]. The MKM follows the linear-quadratic model with α and β coefficients for dose and the square of the dose, respectively. The MKM is written as follows

$$\ln(SF) = \alpha D + \beta D^2 \quad (13)$$

$$\alpha_p = \alpha_x + \beta_x \frac{\overline{y_D}}{\pi \rho r_d^2} \quad (14)$$

$$\beta_p = \beta_x \quad (15)$$

where SF is the survival fraction, $\overline{y_D}$ is the dose-mean lineal energy, ρ is the mass density of water and the subscripts p and x denote protons and x-rays, respectively. The MKM assumes that regardless of the radiation type, the β term is constant. The MK model assumes that α_0 is the slope of the survival curve in the limit of $LET = 0$, but in this work, α_x is used rather than α_0 , as the reference radiation α parameter. LET for the reference radiation is assumed to be low enough that α variations for the reference radiation is negligible, making α_0 appropriate.

2.3 Calculating $\overline{y_D}$ and fitting MKM to experimental data

To input microdosimetric values such as $\overline{y_D}$ into the MKM, they must be measured, such as with a tissue-equivalent proportional counter (TEPC) or calculated. This subchapter will propose a method to calculate $f(y)$ using the Geant4 DNA toolkit. Then a method to calculate $\overline{y_D}$ based on the proton energy spectrum and lineal energy probability density functions ($f(y)$) will be presented. Finally the least-squares fitting of the MK model to experimental data will be described.

2.3.1 Computational Resources

All Monte Carlo and Matlab computations done in this work were performed on either the Nautilus or Seadragon clusters at the MD Anderson Cancer Center. The Nautilus cluster had over 300 compute nodes, and each node was a BL465c G7 blade with two 12-core AMD 6174 processors, for a total of 12 cores per node. Each code had at minimum, 64 GB RAM.

Nautilus's operating system was Red Hat Enterprise Linux 6.5 with a queueing interface consisting of PBS/Torque and Moab. Seadragon is MD Anderson's newest cluster, consisting of

204 compute nodes with 27 CPU cores per node, and 192 GB RAM per node. Seadragon uses Red Hat Enterprise 7.4 as its operating system and uses the Spectrum Load Sharing Facility 10.1 software for job scheduling.

2.3.2 Geant4 DNA

The DNA extension to the Geant4 Monte Carlo simulation toolkit is designed to enable modeling of ionizing radiation at the scale of DNA in liquid water [6, 33-36]. In order to model radiation interactions with matter on the scale of nanometers, unique particle physics models have been developed for increased accuracy at low energies, on the order of hundreds of eV. These models are essential to calculate the energy loss of protons at low, although relevant energies for proton therapy around 1 MeV. As with any Monte Carlo system, the settings for the simulation are important. This work used all the default settings provided in the Geant4 DNA 10.2.0 release, except for the secondary particle range cut value. This range cut refers to the minimum range a secondary particle must have in order to be transported by the Monte Carlo code. If an ionized electron has a range below the cut value the electron and all its kinetic energy is deposited locally without being transported. For protons with kinetic energies > 2 MeV, the cut length was left at 1000 nm. For protons ≤ 2 MeV the cut length was set to 5 nm. The different cut lengths will be explained in section 2.3.3. Simulations were created to transport protons through a cube of liquid water with 5 μm side lengths. 295 proton energies were simulated, with up to 100 unique tracks simulated per energy. The range of energies for protons was [0.1, 223] MeV, which covered the energy spectrum of the proton machine at the Proton Therapy Center Houston. The output of the simulation included, for all primary and secondary particles, the position in 3 dimensions, kinetic energy, event type, and parent track. This allowed the reconstruction of the path and kinetic energy of the primary proton through the

water cube, as well as the path and kinetic energies of all ionized electrons and other secondary particles.

2.3.3 Calculating y and $f(y)$

A Matlab script was developed to take the output of the Geant4 DNA and reconstruct the 3D map of the proton's track through the water cube, along with the position and energy of secondary particles. The script placed spheres with radii of 500 nm at random points at and along the proton track. The script determined if energy was deposited into a sphere, and how much, computing ε from Eq. 8. The mean chord length \bar{l} was calculated via Cauchy's formula to be

$$\bar{l} = 4(V/S) \quad (16)$$

where V is the volume and S is the surface area of the sphere. Thus for each randomly-placed sphere the lineal energy deposited in that sphere was calculated. The scored y values were then binned, with a range of [0.01, 300] keV/ μ m and 0.1 keV/ μ m bin widths. The result of these binned lineal energy values is a histogram, which is the function $f(y)$ for that proton energy. Because the y values scored n times were used to compute $\overline{y_D}$, which is a sum over all scored values according to Eq. 12, the fractional error in each bin was assumed to follow a Poissonian distribution:

$$Error = \frac{\sqrt{n \text{ samples}}}{n \text{ samples}} \quad (17)$$

The total fractional error for the $f(y)$ of a single proton energy was the quadrature sum of the fractional error of each lineal energy bin. The total number of scored spheres were increased

until the total maximum fractional error for any $f(y)$ was $< 1.5 \times 10^{-4}$ for protons < 100 MeV. For protons with energies > 100 MeV the number of samples per track was set to 500.

For protons with energies > 2 MeV, the vast majority of ionized electrons had kinetic energies that enabled them to travel further than 1000 nm, the default cut length in the Geant4 DNA “dnaphysics” example. However for protons $\lesssim 2$ MeV, a significant fraction of ionized electrons did not have enough kinetic energy to go beyond 1000 nm, but did have enough energy to travel beyond the 500 nm radius of the domain, and thus the Geant4 code deposited the kinetic energy of the particle locally. The result of using the 1000 nm cut length for protons with energies ≥ 2 MeV were $\overline{y_D}$ values that were 2-3 times greater than what was expected, based on previously published work by Nikjoo et al and Lindborg et al [37] [38]. Based on these results, all track files for proton energies ≥ 2 MeV were re-simulated and the lineal energy and $f(y)$ re-calculated. The resulting $\overline{y_D}$ values then agreed much closer to Nikjoo et al and Lindborg et al’s values.

2.3.4 Calculating $\overline{y_D}$ of a polyenergetic proton beam

The rate that an ion loses kinetic energy in a micrometer sized volume is not constant. Rather, it follows a probability distribution $f(y)$. This stochastic nature of energy loss must be accounted for in microdosimetry, hence the use of averaged quantities such as $\overline{y_D}$. In the case of a proton beam passing through a patient, particularly at the Bragg peak, the $\overline{y_D}$ value includes energy loss characteristics of a broad energy distribution. It is with this understanding that the following method for calculating $\overline{y_D}$ was conceived. For each energy i , by weighting the constituent $f(y)_i$ by its fluence $\Phi(E)_i$ at a particular point, the probability density function of a polyenergetic proton beam ($f_w(y)$) can be calculated by Eq. 18.

$$f_w(y) = \frac{\sum_i \Phi(E)_i f(y)_i}{\sum_i \Phi(E)_i} \quad (18)$$

The $\overline{y_D}$ of a polyenergetic proton beam is thus:

$$\overline{y_D} = \frac{\int y^2 f_w(y) dy}{\int y f_w(y) dy} \quad (19)$$

2.4 Fitting r_d and calculating RBE

Once $\overline{y_D}$ was calculated, the radius of the domain r_d from Eq. 14 was varied to reach the best agreement with the experimental RBE. The best r_d was found using the least squares method when RBE is modeled as a function of $\overline{y_D}$. The value of r_d was expected to vary by only 200-300 nm at most, and such a difference in the domain size compared to the calculated $\overline{y_D}$ using $r_d = 500$ nm via Geant4 DNA will not change the underlying $f(y)$ distribution significantly. Thus it was appropriate to use the $f(y)$ values calculated with Geant4 DNA. To calculate the RBE of the MK model Eq. 20 was used:

$$RBE = \frac{\sqrt{\alpha_x^2 - 4\beta_x \ln SF} - \alpha_x}{\sqrt{\alpha_p^2 - 4\beta_p \ln SF} - \alpha_p} \times \frac{\beta_p}{\beta_x} \quad (20)$$

The subscripts p and x in Eq. 20 refer to proton and X-ray α and β parameters, respectively.

α_p and β_p are calculated from Eq. 14 and 15, and α_x and β_x are from the LQ fitting parameters of the reference X-ray radiation. SF refers to the survival fraction of the clonogenic cell survival experiments, and was set to 0.1 in this work. Eq. 20 was obtained by solving for the dose terms in the LQ equations and taking the ratio of those doses according to Eq. 1.

2.5 Comparing RBE models

The hypothesis of Specific Aim One was phenomenological RBE models will under-predict RBE by 20% in the Bragg peak and distal falloff region. The percentage difference between the RBE model and experimental data was calculated by Eq. 21:

$$\% \text{ error} = \frac{\text{experimental} - \text{theoretical}}{\text{theoretical}} \times 100 \quad (21)$$

The generic RBE model in Eq. 7 uses LET_D as a measure of radiation quality. Authors such as Mohan et al [12] and Grün et al [11] have argued that dose-averaged LET may not be the most reliable indicator of biological effect. They argue that in theory, for a proton beam with a broad energy distribution such as that found near and distal to the Bragg peak, the low energy (and thus high LET) portion of the proton energy spectrum will kill cells more efficiently than the higher energy (and thus lower LET) portion. Averaging LET values based on dose could lead to breakdowns in the assumed linear relationship between LET and RBE. A comparison of MKM, with its radiation quality measured by $\overline{y_D}$ and the generic RBE model with radiation quality in LET_D would be useful to determine if one model is superior to the other. The Akaike Information Criterion (AIC) analysis method quantitatively compared the MKM with the generic RBE model. AIC analysis compares two models used to fit data and determines which of the two models fits better based on their respective sum of squares. Eq. 22 and Eq. 23 express how the relative likelihood (RL) that the worse-fitting model better represents the data is calculated. The terms $SS1$ and $SS2$ are the sum of squares from each model fit. The values for $SS1$ and $SS2$ were chosen so that $SS2 > SS1$. In Eq. 22 N is the number of experimental RBE points to compare the models to.

$$\Delta AIC = N \times \ln\left(\frac{SS2}{SS1}\right) \quad (22)$$

$$RL = \exp(-\Delta AIC/2) \quad (23)$$

2.6 matRad

MatRad is a treatment planning system written in Matlab [39]. It enables the user to create optimized radiotherapy treatment plans with photons and ions such as protons and carbon. MatRad includes functions for a graphical user interface (GUI), to import DICOM CT data, to optimize treatment plans based on dose objectives, and for carbon ions, it includes a biological optimization option which uses the LEM IV model [40]. A screenshot of the matRad GUI is shown in Fig. 2. Due to being written in Matlab the entire code is open source and the user can modify the underlying functions as they wish. MatRad also supports users creating their own beamlines. For this work, the matRad code used for this work was downloaded on April 5, 2018. Matlab R2017b was used to run matRad. The scanning beamline in use at PTCH, known as G3, was commissioned into matRad. The data for G3 was taken from Monte Carlo data that was validated against measurements. G3 has 94 proton beam energies, from 72.5 MeV to 221.8 MeV, corresponding to ranges of 4 cm to 30.6 cm [41].

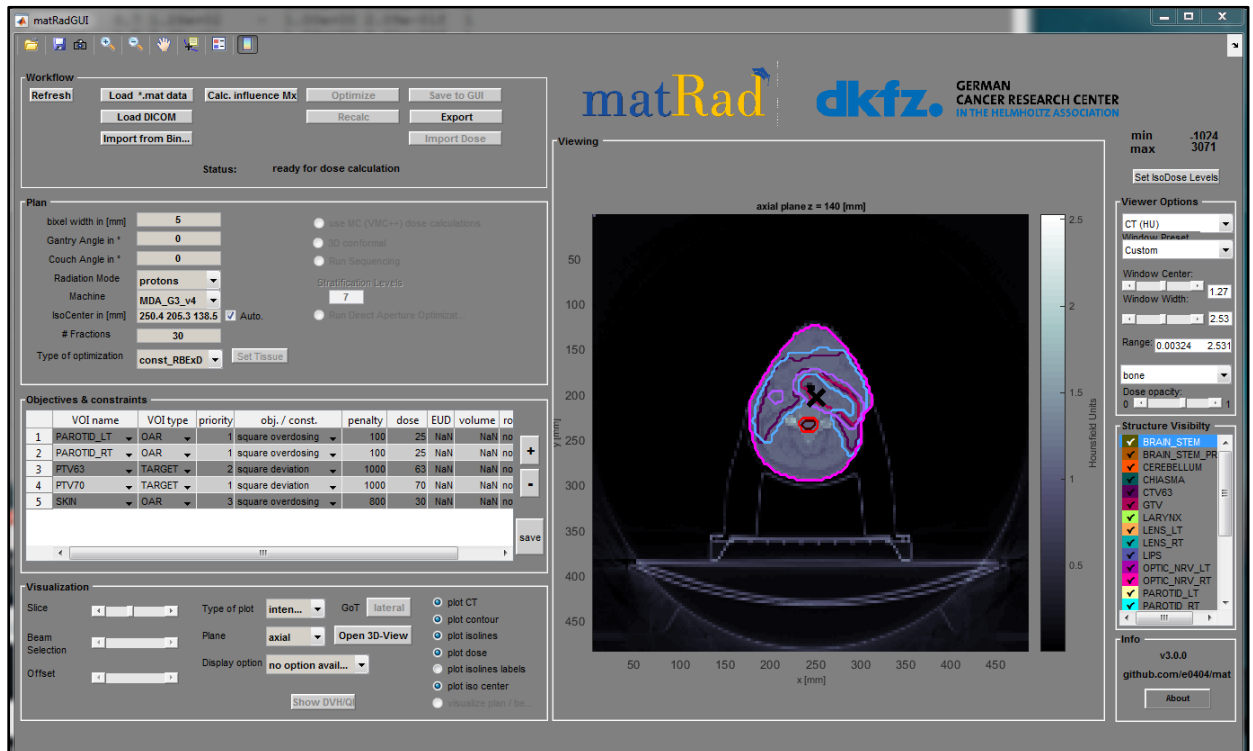


Figure 2: matRad GUI

MatRad has many of the basic functionalities of commercial treatment planning systems, including defining optimization settings. The treatment plan shown comes standard with the matRad download.

There are significant concerns for brainstem toxicities in patients with ependymoma receiving proton radiotherapy [13-15]. In theory, the smaller the $(\alpha/\beta)_x$ ratio is, the greater the RBE [2, 23]. As expressed by Lühr et al, tissues most affected by variable RBE should be late responding tissues (low $(\alpha/\beta)_x$ ratio) that receive low to intermediate doses and are located distal to the target [42]. The brainstem is just such a critical structure and thus, an ependymoma patient planning CT would make an ideal test case to investigate the efficacy of optimizing treatment plans using a variable RBE.

2.6.1 Incorporating MKM optimization into matRad

The MK model requires the calculation of $\overline{y_D}$ to compute α_p and therefore RBE (Eqs. 12, 14, 20). Based on the number of voxels in a modern treatment planning CT ($\sim 10\text{-}20 \times 10^6$) it

is not computationally feasible to compute the proton energy spectrum in each voxel and apply Eq. 19 to calculate RBE during the optimization process, which can require hundreds of RBE×Dose calculations. Therefore the method to calculate RBE by Inaniwa et al for carbon beam therapy in Japan was adopted for this work [43]. In their paper, Inaniwa et al adopted the MK model proposed by Kase et al by calculating z_{1D}^* , or the saturation-corrected dose mean specific energy of the domain delivered in a single event [32]. Carbon ion therapy requires a saturation correction for LETs $> \sim 150$ keV/ μm , where RBE reaches a maximum and further increases in LET result in a decreasing RBE, called the overkill effect. This overkill effect is not present in proton therapy and therefore there needs to be no saturation correction for a treatment planning system using the MK model for proton therapy. In the paper by Inaniwa et al z_{1D}^* was calculated by combining the contributions from individual carbon beamlets:

$$(z_{1D}^* \text{ mix})_i = \frac{\sum_{j=1}^{N_{spot}} w_j \cdot d_{ij} \cdot (z_{1D}^*)_{ij}}{\sum_{j=1}^{N_{spot}} w_j \cdot d_{ij}} \quad (24)$$

where $(z_{1D}^*)_{ij}$ is the saturation-corrected dose mean specific energy of the domain at position i delivered by beam j , and N_{spot} is the number of beam spots in the treatment plan. w_j represents the weight of spot j and d_{ij} is the dose at point i from beam j . During optimization, the values of w_j are varied to achieve target coverage and organ at risk (OAR) sparing. The approach implemented into matRad followed this same calculation in Eq. 24, except $\overline{y_D}$ was calculated instead of z_{1D}^* . From Kase et al, z_{1D} (the dose mean specific energy, not saturation corrected) is related to $\overline{y_D}$ by:

$$z_{1D} = \frac{\overline{y_D}}{\rho \pi r_d^2} \quad (25)$$

where r_d is the radius of the domain. In this work the dose mean lineal energy of a mixed proton field at position i with the number of spots N_{spot} and beam j was calculated by Eq. 26.

$$(\overline{y_{D_{mix}}})_i = \frac{\sum_{j=1}^{N_{spot}} w_j \cdot D_{ij} \cdot (\overline{y_D})_{ij}}{\sum_{j=1}^{N_{spot}} w_j \cdot D_{ij}} \quad (26)$$

In matRad the dose to a point i from pencil beam j is calculated by the matrix multiplication of the dose influence matrix D_{ij} and the weight w of pencil beam j . Casting this as a matrix vector product $\vec{d} = D\vec{w}$ takes advantage of Matlab's speed in matrix multiplication, where \vec{d} is the a vector with the dose to every voxel, from every beam. Therefore including the $(\overline{y_D})_{ij}$ term in Eq. 26 was conceptually straightforward.

To implement the $\overline{y_{D_{mix}}}$ calculation, the $\overline{y_D}$ at each depth for every proton beam energy must be calculated. To do this, the proton energy spectrum at 1 mm intervals in depth, for all 94 beams in G3 was simulated using a MCNPX model of the beamline [44]. The $\overline{y_D}$ at every mm was calculated using Eq. 18 and Eq. 19, using the $f(y)$ calculated from Geant4 DNA simulations presented in sections 2.3.2 and 2.3.3. The results of these calculations were saved in a file called `yD_table_MDA_G3.mat` for later use in calculating $\overline{y_D}$ at a given depth for every beam energy. Figure 3 shows a screenshot of the `yD_table_MDA_G3.mat` data. The public version of matRad does not currently feature the ability to incorporate variable RBE in proton treatment plan optimization. However this functionality was added by modifying the matRad source code. In the default dose calculation function called `matRad_calcParticleDose.mat`, the dose from every pencil beam to every voxel in the planning CT is calculated. By default, this data is not available to the user, as the total dose to all voxels from all beams is the output of the function. A copy of `matRad_calcParticleDose.mat` called `matRad_calcParticleDose_MKM_optimization.mat` was created in order to save, as output, the dose from each pencil beam to each voxel. This enabled the separation of each pencil

yD_table				
1x94 struct with 4 fields				
Fields	Energy	max_depth	yD_vec	depthVec
1	146.9000	154.5000	1x300 double	1x300 double
2	148.8000	158.5000	1x300 double	1x300 double
3	72.5000	42.5000	1x300 double	1x300 double
4	221.8000	315.5000	1x350 double	1x350 double
5	76.1000	46.5000	1x300 double	1x300 double
6	77	47.5000	1x300 double	1x300 double
7	77.9000	48.5000	1x300 double	1x300 double
8	78.8000	49.5000	1x300 double	1x300 double
9	79.7000	50.5000	1x300 double	1x300 double
10	121.2000	109.5000	1x300 double	1x300 double
11	80.5000	51.5000	1x300 double	1x300 double
12	81.4000	52.5000	1x300 double	1x300 double
13	82.2000	53.5000	1x300 double	1x300 double
14	83.1000	54.5000	1x300 double	1x300 double
15	83.9000	55.5000	1x300 double	1x300 double

Figure 3: yD_table_MDA_G3.mat format

This data table enables the calculation of $\overline{y_D}_{mix}$ for the G3 beamline. $\overline{y_D}$ values as a function of depth are interpolated based on this data. There is also an entry for the maximum depth of the beam. All $\overline{y_D}$ values beyond this depth are set to 0.

beam's contribution to the total dose in a voxel, which is used in Eq. 26. During the optimization process, the vector of weights (w_j) of each pencil beam j was varied until the dose constraints and objectives were solved to an acceptable level. For each iteration the function `matRad_calcParticleDose_MKM_optimization.mat` was called because as the pencil beam weights changed, each pencil beam's dose contribution to a voxel changed. The process to recalculate the dose contributions from each pencil beam to each voxel takes approximately two to four minutes, and is a major contributor to the slowness of the MKM optimization process in `matRad`.

The MKM optimization functionality written into `matRad` is summarized as follows.

Inside the optimization function, a function called `matRad_backProjection.mat` is called to calculate the current dose distribution, which is then evaluated via the optimizer's objective function for conformity to plan constraints and objectives. `matRad_backProjection.mat` calls `MKM_RBE_Calculator.mat` which then calls `matRad_calcParticleDose_MKM_optimization.mat`, which calculates the dose contribution from each pencil beam to every voxel. The output of this function is a data structure called `dij_MKM`. This is then used as input into a function called `yD_doseAvg_calculation_beams.mat` was written to calculate $(\overline{y_{D_{mix}}})_i$ according to Eq. 26. This function in turn called `calculateProtonRBEFromyD.mat`, a function written to calculate the RBE in all voxels of the planning CT. The output of `calculateProtonRBEFromyD.mat` is a matrix named `MKM_RBE_cube` with dimensions $X \times Y \times Z$, where X , Y , and Z are the number of voxels in the planning CT in the respective coordinate axes. `MKM_RBE_cube` was then multiplied by the physical dose distribution to get the RBE-weighted dose (RWD) distribution. The RWD distribution was then evaluated for adherence to the dose constraints and objectives. This process was repeated until the dose constraints and objectives were met. Fig. 4 is a flowchart of the optimization process. For this project `MKM_RBE_Calculator.mat`, `yD_doseAvg_calculation_beams.mat` and `calculateProtonRBEFromyD.mat` were newly written functions, while `matRad_backProjection.mat` and `matRad_calcParticleDose_MKM_optimization.mat` were functions provided by `matRad` that were modified to perform variable RBE optimization.

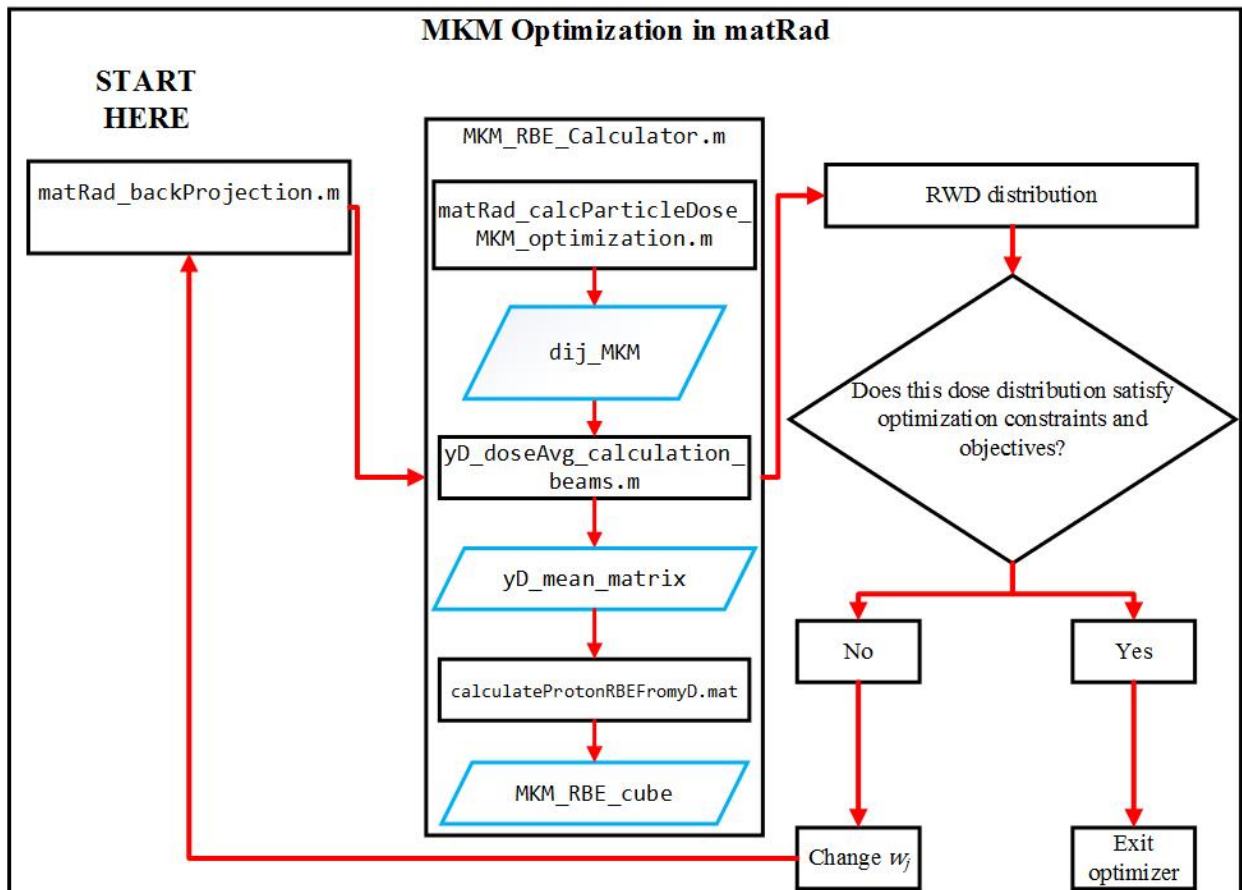


Figure 4: RBE optimization implemented into matRad.

This flowchart demonstrates the implementation of calculating RBE via the MK model in matRad. Functions called by the optimization process end in .m, and are shown in black rectangles. The output of these functions are shown as blue parallelograms.

2.6.2 Patient data

As presented in section 1.2 and Refs 13-15, there are significant concerns about brainstem toxicities with pediatric ependymoma patients. The treatment planning CT from a patient treated at the PTCH was used to evaluate the clinical effect of incorporating variable RBE as calculated by the MK model into intensity modulated proton therapy (IMPT) treatment plans. The patient was treated on the G3 scanning beamline. The OAR and target contours and simulation CT were imported into matRad. The beam angles chosen in matRad were identical to those used for treatment at PTCH, and consisted of three beams. Gantry angles were 110°, 180°

and 250°, and the couch angle for each beam was 0°. The distance between spots was set to 9 mm. Planning objectives in matRad were guided by constraints given in Table 2. The GTV was prescribed 1.8 Gy(RBE) per fraction for 30 fractions, for a total target prescription of 54 Gy(RBE) to the GTV. The constraints and dose prescriptions are the same as those used by a current MD Anderson internal trial for ependymoma patients.

Table 2: Organ at risk constraints for ependymoma patients.

OAR	Constraint
Optic nerves (ON)	Max ≤ 55 Gy(RBE)
Optic chiasm (OC)	Max ≤ 55 Gy(RBE)
Brainstem	D10% < 55.4 Gy(RBE) D50% < 52.4 Gy(RBE) V50 $< 61.7\%$ V55 $< 17.7\%$ D0.1cc < 56.6 Gy(RBE)
Spinal cord	Max ≤ 50 Gy(RBE)
Eye, including retina	Max 45 Gy(RBE)

Once all the dose constraints were met, and the GTV received as close to 100% of the 54 Gy(RBE) prescription dose as possible without exceeding OAR tolerance doses, the treatment plan was deemed acceptable for MKM optimization. The equivalent uniform dose (EUD) to the brainstem was then calculated and the normal tissue complication probability (NTCP) computed, using the parameters outlined in section 2.6.3.

2.6.3 Radiobiological properties of tissues during MKM optimization

The α_0 and β values for each tissue were the same ones assigned by Frese et al in their RBE analysis, which was taken from a PhD dissertation by Cronqvist [45, 46]. α_0 is used rather than α_x to be consistent with the MKM laid out by Kase et al, where α_0 is the initial survival curve slope in the limit of LET=0. The α_0 values presented by Frese are corrected from the α_x values by assuming LET in the experiments from which α_x was determined is approximately

0.5 keV/ μm . Using either α_0 or α_x is assumed to have a negligible effect on the RBE value.

Therefore the α/β ratios given in Table 3 are not exactly 10 Gy or 2 Gy, but slightly less.

However the α_x/β_x ratio given by Frese are exactly 10 Gy or 2 Gy. The value for r_d in the GTV and CTV was set to 243 nm. This was chosen based on the fitted value for the AGO1522 cell line in the SOBP irradiations. AGO1522 has an α/β ratio of 8.7 Gy, which is the closest experimental value to the assumed tumor α/β ratio of 10 Gy. For all other tissues, since they have an α/β ratio of 2 Gy, r_d was set to 461 nm. This is also based on fitting a cell line, in this case the U87 SOBP experiment, as the U87 α/β ratio is 1.83 Gy. Table 3 gives the assumed parameters used during RBE calculations in this work.

Table 3: Radiobiological properties of tissues for RBE optimization

Tissue	α/β (Gy)	α_0 (Gy ⁻¹)	β (Gy ⁻²)
Tumor (GTV, CTV)	10	0.1084	0.0112
Brainstem	2	0.0492	0.0266
Spinal cord	2	0.0367	0.0203
Optic nerves	2	0.0256	0.0471
Optic chiasm	2	0.0256	0.0471
Eyes	2	0.0367	0.0203
Brain	2	0.0580	0.0310

To estimate the normal tissue complication probability (NTCP) for the brainstem, equivalent uniform dose (EUD) and Niemierko's NTCP/TCP model was used [47] [48]. EUD is calculated by

$$EUD = \left(\sum_{i=1} (v_i D_i^a) \right)^{\frac{1}{a}} \quad (27)$$

where v_i is the i 'th volume receiving dose D_i , and a is a unitless parameter that corresponds to the tumor or normal tissue. NTCP is calculated by

$$NTCP = \frac{1}{1 + \left(\frac{TD_{50}}{EUD} \right)^{4\gamma_{50}}} \quad (28)$$

In Eq. 28, TD_{50} corresponds to the tolerance dose that results in 50% of a population experiencing a complication, and γ_{50} is a parameter that describes the slope of the dose-response curve, and is unique to each tissue. Using the NTCP/TCP tool published by Gay and Niemierko, brainstem EUD and NTCP were calculated [49]. Setting the a parameter in the EUD calculation to a large positive number will skew the EUD towards the maximum dose to a structure. The maximum dose is important to a serial organ such as the brainstem, as the most difficult planning constraint to meet is to keep the dose to 0.1 cc of the brainstem below 56.6 Gy(RBE). Thus for brainstem EUD, the $a = 25$. As recommended by Niemierko, γ_{50} was set to 4 and TD_{50} was set to 65 Gy [49].

2.6.4 Comparing standard treatment plans to MKM optimized plans

To assess the impact of including variable RBE during treatment plan optimization, a treatment plan optimized using the standard RBE=1.1 paradigm was compared to a treatment plan optimized using the MK model for variable RBE. A radiation oncologist reviewed these plans and deemed them clinically realistic. Treatment plan DVHs and NTCPs for the brainstem will be compared. There will be three DVHs and three NTCPs; one each from the std_opt, std_opt_MKM_calc, and MKM_opt plans. These plans are defined in the workflow below:

- 1) Patient planning CT, OARs and target contours are imported into matRad. Optimization objectives are also set.
- 2) A treatment plan assuming a constant RBE=1.1 is created and optimization objectives varied until OAR constraints are met and the plan is approved by a radiation oncologist as clinically realistic. This standard treatment plan is saved and is known as the std_opt plan.
- 3) The variable RBE using MKM is calculated on std_opt. The variable RBE result is then saved as well. This is known as the std_opt_MKM_calc plan.
- 4) The variable RBE, MKM-calculated standard treatment plan (std_opt_MKM_calc) is used as the starting point for an MKM-optimized treatment plan. This resulting MKM-optimized plan is then saved. This plan is known as the MKM_opt plan.

One purpose of this workflow was to first create a realistic treatment plan with the RBE=1.1 model (std_opt) and then calculate the variable RBE and RWD (std_opt_MKM_calc) to evaluate the potential dangers in using a constant RBE. RWD hot spots are expected in critical structures such as the brainstem and spinal cord, and in normal brain tissue. The second purpose of this workflow was to take the std_opt_MKM_calc plan and optimize it using a variable RBE calculated via the MK model. It is hypothesized that by including the MK model in the optimization algorithm, another clinically realistic treatment plan can be created (MKM_opt) that should both increase target coverage and reduce normal issue toxicity as compared to the std_opt_MKM_calc plan.

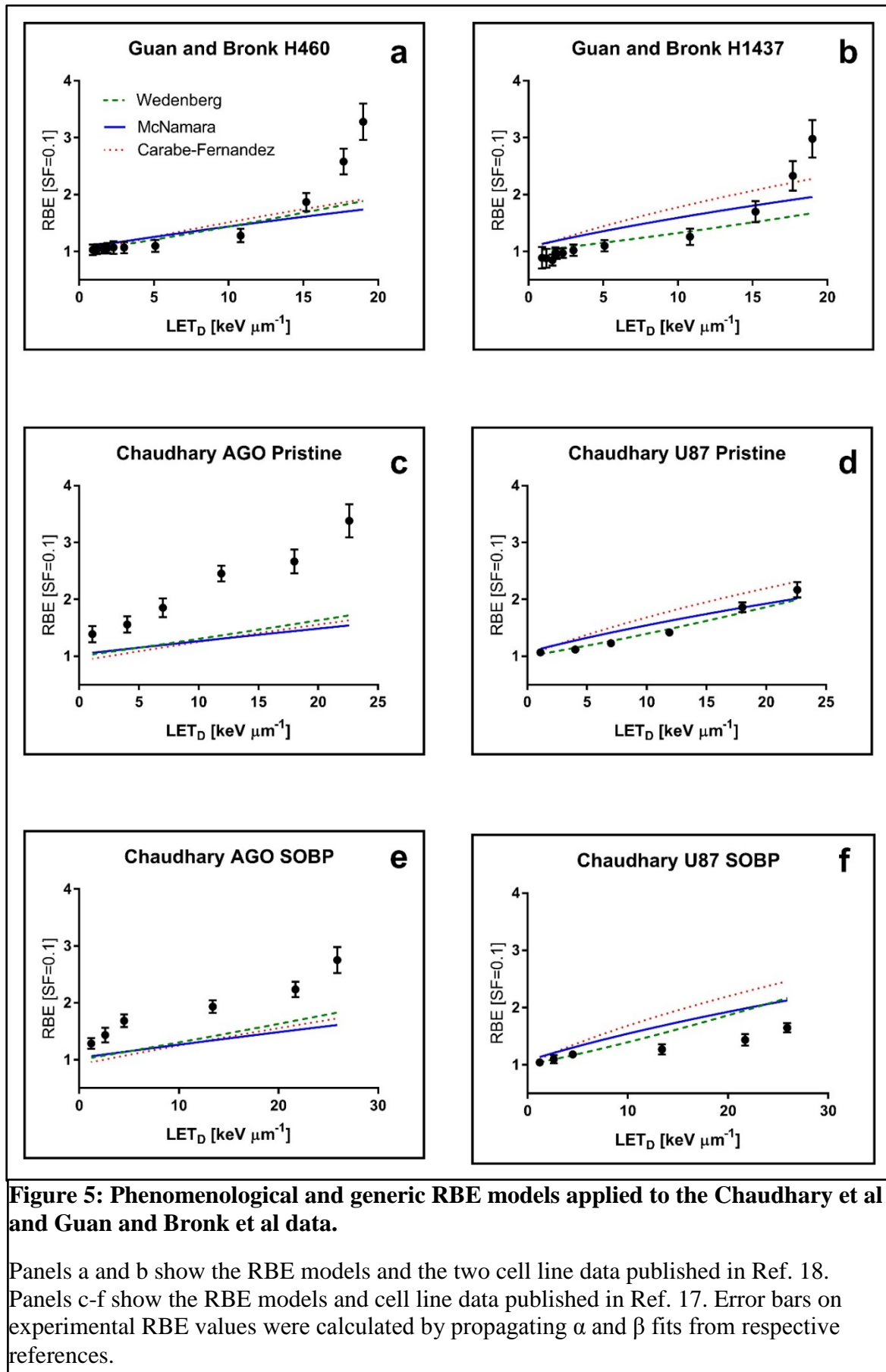
Chapter 3: Results

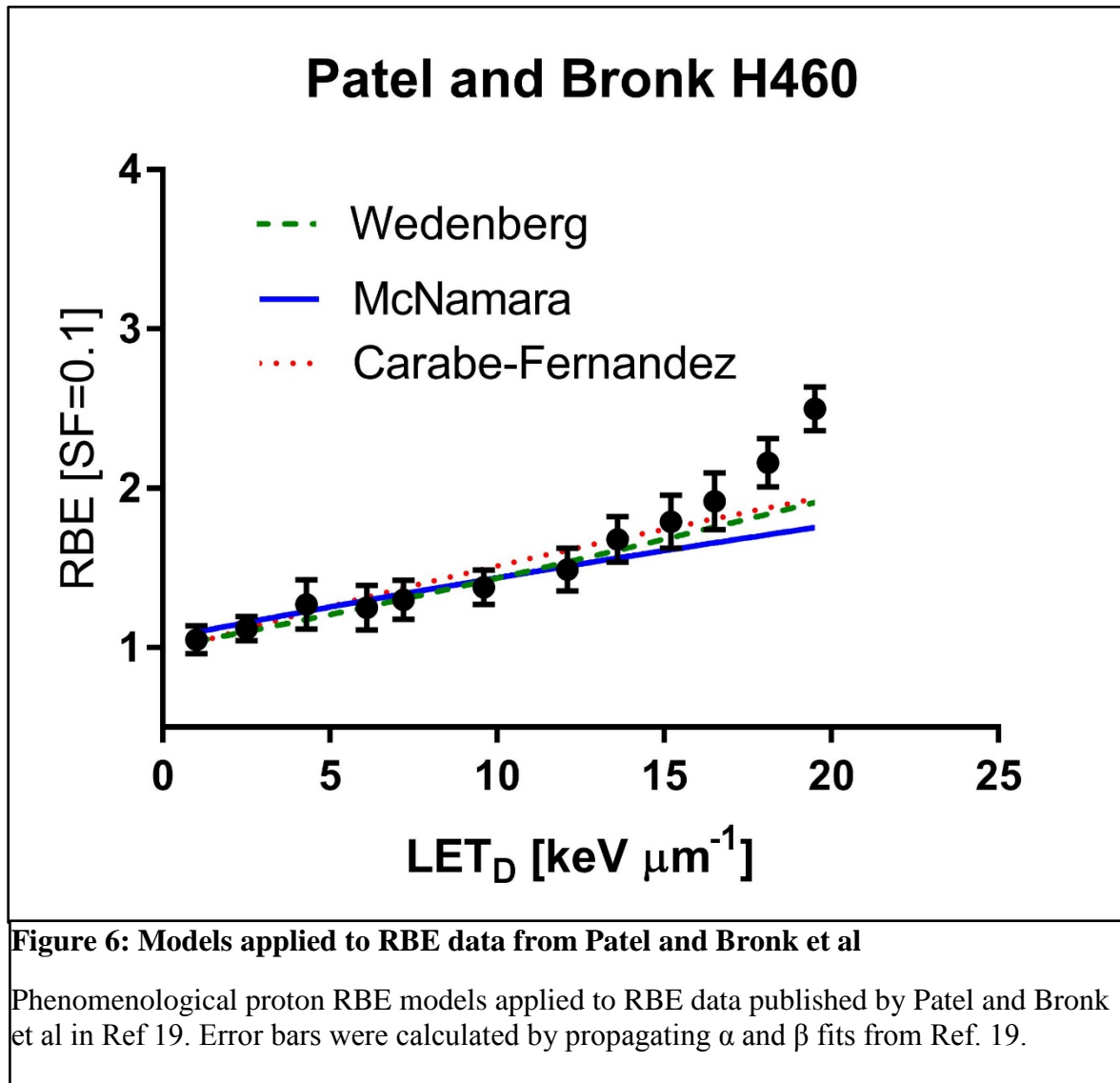
This chapter is based upon a paper reprinted from International Journal of Radiation Oncology*Biology*Physics, Vol. 104, Issue 2, Mark Newpower, Darshana Patel, Lawrence Bronk, Fada Guan, Pankaj Chaudhary, Stephen J. McMahon, Kevin M. Prise, Giuseppe Schettino, David R. Grosshans, Radhe Mohan, Using the Proton Energy Spectrum and Microdosimetry to Model Proton Relative Biological Effectiveness, Pages 316-324. Copyright 2019 with Permission from Elsevier. 2019,ISSN 0360-3016, <https://doi.org/10.1016/j.ijrobp.2019.01.094>.

(<http://www.sciencedirect.com/science/article/pii/S0360301619301853>)

3.1 Phenomenological model fitting to experimental RBE data

The phenomenological models proposed by Wedenberg et al [21], Carabe-Fernandez et al [22], and McNamara et al [24] were applied to the RBE datasets previously published by Chaudhary et al [17], Guan and Bronk et al [18] and Patel and Bronk et al [19]. The LQ model parameters used for each cell line are given in Table 1. Fig. 5 shows the RBE models with the data from Guan and Bronk et al and Chaudhary et al. Fig. 6 shows the RBE models with the data published by Patel and Bronk et al.





3.2 Difference between phenomenological RBE models and RBE data

The Bragg peak in the Guan and Bronk et al data occurs near the $LET_D = 10.8 \text{ keV}/\mu\text{m}$ data point, meaning the four highest LET values are in the Bragg peak and distal falloff regions. Tables 4 and 5 show the results of the phenomenological models' accuracy in modeling the data from Guan and Bronk et al.

Table 4: Guan and Bronk et al H460 data compared to phenomenological RBE models.

The predicted RBE values for each of the three phenomenological RBE models are given, as well as the percent difference between the models and experimental RBE. A percent difference > 0 means the RBE model under-predicted RBE. Abbreviations: LET: linear energy transfer, units of keV/ μm ; Exp. RBE: Experimental RBE; Wed: Wedenberg RBE model; McN: McNamara RBE model; CF: Carabe-Fernandez RBE model.

LET _D	Exp. RBE	Wed	% diff from Exp. RBE	McN	% diff from Exp. RBE	CF	% diff from Exp. RBE
10.8	1.28	1.48	-14%	1.47	-13%	1.53	-16%
15.2	1.87	1.69	11%	1.61	16%	1.72	9%
17.7	2.58	1.81	43%	1.69	53%	1.82	42%
19	3.28	1.89	74%	1.74	89%	1.87	75%

Table 5: Guan and Bronk et al H1437 data compared to phenomenological RBE models.

The predicted RBE values for each of the three phenomenological RBE models are given, as well as the percent difference between the models and experimental RBE. A percent difference > 0 means the RBE model under-predicted RBE. Abbreviations: LET: linear energy transfer, units of keV/ μm ; Exp. RBE: Experimental RBE; Wed: Wedenberg RBE model; McN: McNamara RBE model; CF: Carabe-Fernandez RBE model.

LET _D	Exp. RBE	Wed	% diff from Exp. RBE	McN	% diff from Exp. RBE	CF	% diff from Exp. RBE
10.8	1.26	1.35	-7%	1.63	-23%	1.78	-29%
15.2	1.7	1.52	12%	1.81	-6%	2.02	-16%
17.7	2.33	1.62	44%	1.91	22%	2.15	8%
19	2.98	1.67	78%	1.69	76%	2.21	35%

In the data from Chaudhary et al, the Bragg peak in the pristine Bragg peak experiments occurs at the LET_D=11.8 keV/ μm data point. Table 6 shows the results of the phenomenological model fittings of the pristine Bragg peak experiments. Chaudhary et al also included RBE experiments done in an SOBP. The most proximal point in the SOBP was where LET_D = 2.6 keV/ μm . The results of phenomenological model fittings for the Chaudhary et al SOBP data are shown in Table 7. The Bragg peak in the Patel and Bronk et al data occurs closest to the LET_D=9.8 keV/ μm point. Table 8 shows the results of the phenomenological RBE model fittings to this data.

Table 6: Chaudhary et al pristine Bragg peak data compared to phenomenological RBE models.

The predicted RBE values for each of the three phenomenological RBE models are given, as well as the percent difference between the models and experimental RBE. A percent difference > 0 means the RBE model under-predicted RBE. Abbreviations: LET: linear energy transfer, units of keV/ μm ; Exp. RBE: Experimental RBE; Wed: Wedenberg RBE model; McN: McNamara RBE model; CF: Carabe-Fernandez RBE model.

Pristine Bragg Peak, AGO1522 Cell Line							
LET _D	<i>Exp. RBE</i>	<i>Wed</i>	<i>% diff from Exp. RBE</i>	<i>McN</i>	<i>% diff from Exp. RBE</i>	<i>CF</i>	<i>% diff from Exp. RBE</i>
11.9	2.45	1.37	79%	1.3	88%	1.3	88%
18	2.66	1.56	71%	1.44	85%	1.48	80%
22.6	3.38	1.72	97%	1.54	119%	1.61	110%
Pristine Bragg Peak, U87 Cell Line							
LET _D	<i>Exp. RBE</i>	<i>Wed</i>	<i>% diff from Exp. RBE</i>	<i>McN</i>	<i>% diff from Exp. RBE</i>	<i>CF</i>	<i>% diff from Exp. RBE</i>
11.9	1.42	1.48	-4%	1.62	-12%	1.75	-19%
18	1.84	1.77	4%	1.85	-1%	2.04	-10%
22.6	2.15	2	8%	2.01	7%	2.25	-4%

Table 7: Chaudhary et al SOBP peak data compared to phenomenological RBE models.

The predicted RBE values for each of the three phenomenological RBE models are given, as well as the percent difference between the models and experimental RBE. A percent difference > 0 means the RBE model under-predicted RBE. Abbreviations: LET: linear energy transfer, units of keV/ μ m; Exp. RBE: Experimental RBE; Wed: Wedenberg RBE model; McN: McNamara RBE model; CF: Carabe-Fernandez RBE model.

SOBP, AGO1522 Cell Line							
LET_D	Exp. RBE	Wed	% diff from Exp. RBE	McN	% diff from Exp. RBE	CF	% diff from Exp. RBE
2.6	1.44	1.08	34%	1.09	32%	1.01	43%
4.5	1.69	1.13	49%	1.13	50%	1.07	58%
13.4	1.93	1.41	37%	1.34	44%	1.35	43%
21.7	2.24	1.69	33%	1.52	47%	1.59	41%
25.9	2.75	1.83	50%	1.61	71%	1.70	61%

SOBP, U87 Cell Line							
LET_D	Exp. RBE	Wed	% diff from Exp. RBE	McN	% diff from Exp. RBE	CF	% diff from Exp. RBE
2.6	1.11	1.09	2%	1.20	-8%	1.20	-8%
4.5	1.18	1.17	1%	1.30	-9%	1.33	-11%
13.4	1.27	1.55	-18%	1.68	-24%	1.82	-30%
21.7	1.44	1.95	-26%	1.98	-27%	2.21	-35%
25.9	1.64	2.17	-24%	2.12	-23%	2.38	-31%

Table 8: Patel and Bronk et al H460 data compared to phenomenological RBE models.

The predicted RBE values for each of the three phenomenological RBE models are given, as well as the percent difference between the models and experimental RBE. A percent difference > 0 means the RBE model under-predicted RBE. Abbreviations: LET: linear energy transfer, units of keV/ μ m; Exp. RBE: Experimental RBE; Wed: Wedenberg RBE model; McN: McNamara RBE model; CF: Carabe-Fernandez RBE model.

LET_D	Exp. RBE	Wed	% diff from Exp. RBE	McN	% diff from Exp. RBE	CF	% diff from Exp. RBE
9.8	1.39	1.43	-2%	1.43	-3%	1.48	-6%
12.3	1.47	1.55	-5%	1.51	-3%	1.59	-8%
13.8	1.75	1.62	8%	1.57	12%	1.66	6%
15.2	1.78	1.69	5%	1.61	10%	1.72	3%
16.8	1.96	1.77	11%	1.66	18%	1.79	10%
18.9	2.20	1.88	17%	1.73	27%	1.87	18%
20.2	2.54	1.95	30%	1.77	43%	1.92	32%

3.3 Fractional error of Geant4 DNA $f(y)$ scoring method

Due to the stochastic nature of energy deposition on the micrometer scale, the method for calculating $f(y)$ for each proton energy as outlined in Chapter 2.3.3 is subject to uncertainty. This uncertainty was quantified with fractional error as expressed in Eq. 17. For this work, 295 proton energies were simulated and their $f(y)$ calculated. The proton energy range for this data set is [0.1, 223.0] MeV, which covers the relevant energy range for proton therapy performed at the PTCH. Fig. 7 shows the fractional error for each calculated $f(y)$ and the number of scored spheres per track to reach that fractional error. Protons with kinetic energies < 100 MeV had a maximum fractional error of 1.5×10^{-4} , while protons with kinetic energy > 100 MeV had a maximum fractional error of 1×10^{-3} .

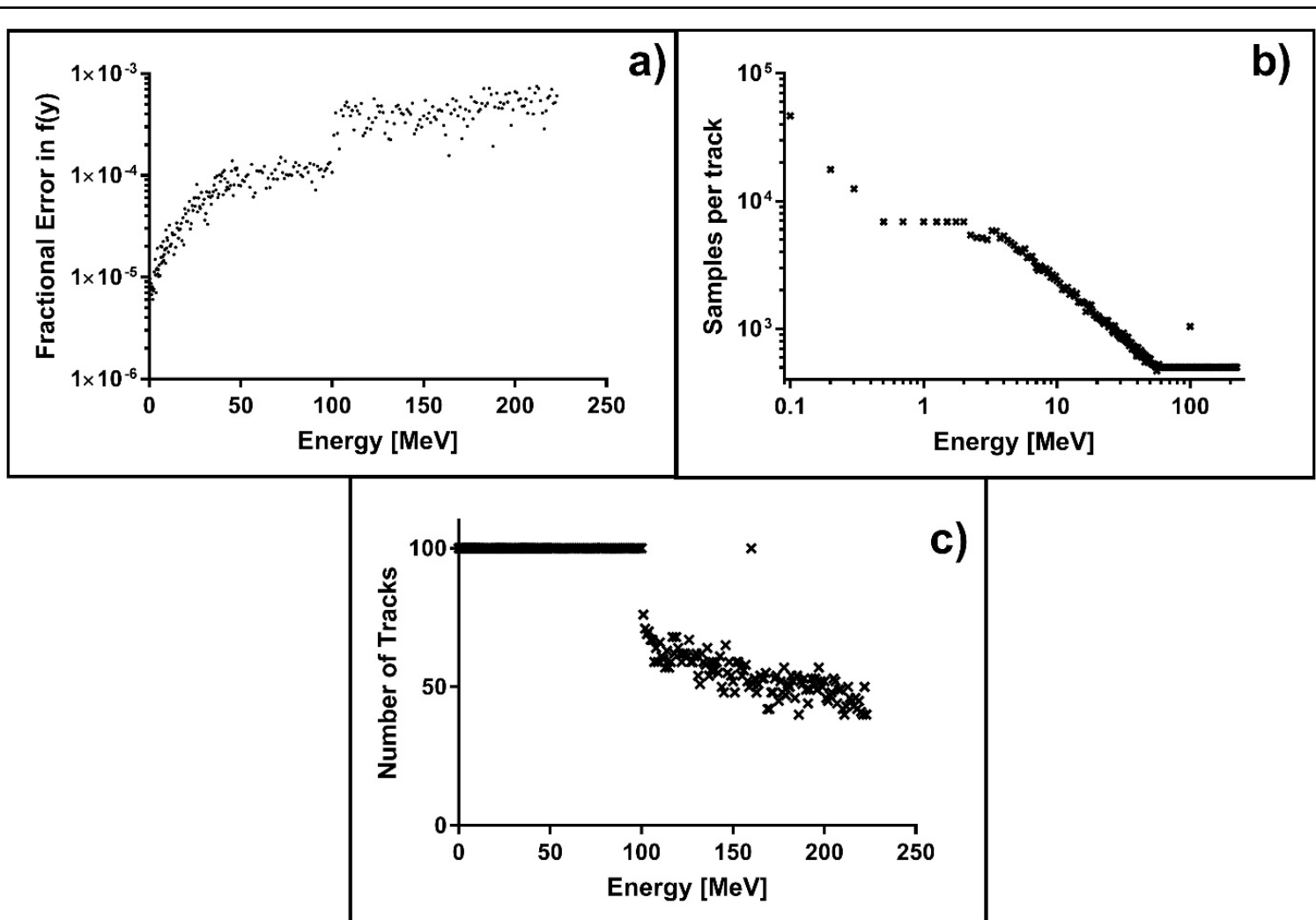


Figure 7: Fractional Error, samples per track, and number of tracks sampled using Geant4 DNA

Panel a) shows the total fractional error in each calculated $f(y)$, by using the number of sampled domains per track, given in panel b). Panel c) shows the total number of tracks used to calculate $f(y)$. The discontinuities at 100 MeV in panels a) and c) are a result of different ionization models used by Geant4 DNA. The transition from one model to another occurs at 100 MeV. Used by permission from Elsevier.

3.4 Calculating $\overline{y_D}$

Fig. 8 shows $\overline{y_D}$ for each of the $f(y)$ calculated via Eq. 19. The plot in Fig. 8 thus represents the calculated $\overline{y_D}$ for a purely monoenergetic proton beam. A comparison of these $\overline{y_D}$ values and those published by Nikjoo et al [37] was made by Newpower et al [50], and they concluded the $\overline{y_D}$ between the two studies were very similar, particularly at low proton energies. The comparison is shown in Fig. 8. In each of the three RBE studies used as experimental data in this work, the authors calculated the proton energy spectrum at each RBE measurement point. These spectra were used as input for Eq. 18 and the dose mean lineal energy ($\overline{y_D}$) was calculated via Eq. 19. The results of these calculations are shown in Fig. 9. The linear relationship between $\overline{y_D}$ and LET_D for each beam configuration is shown in each panel.

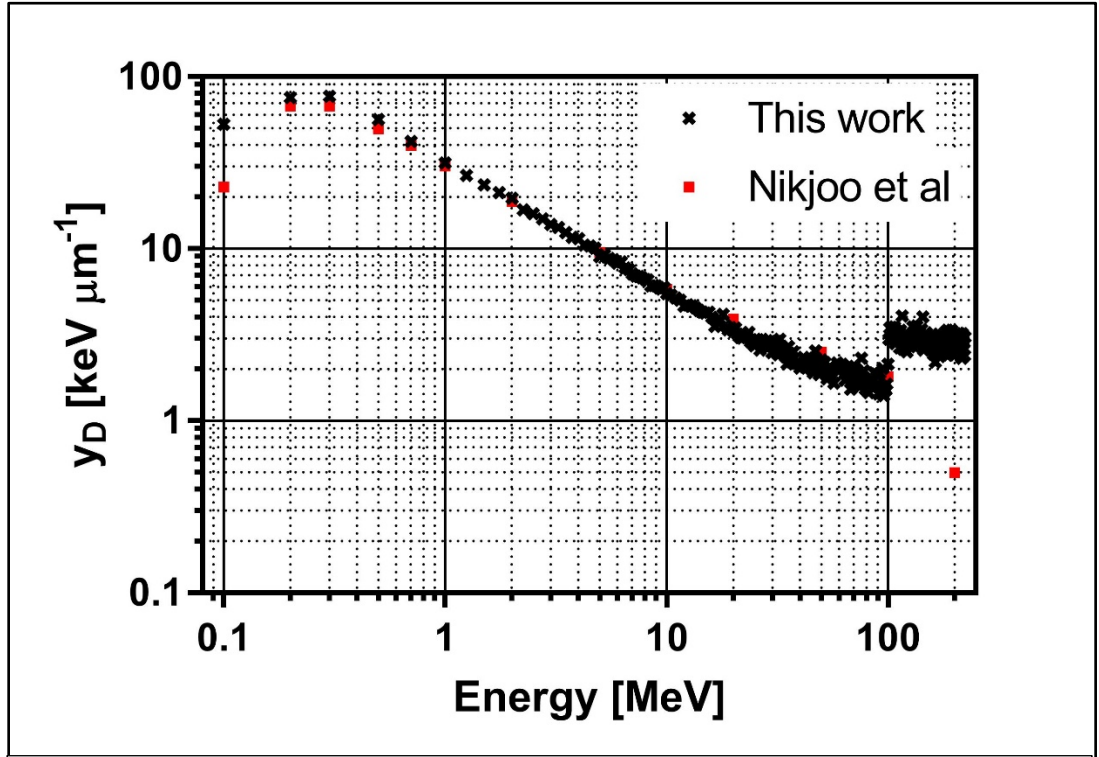
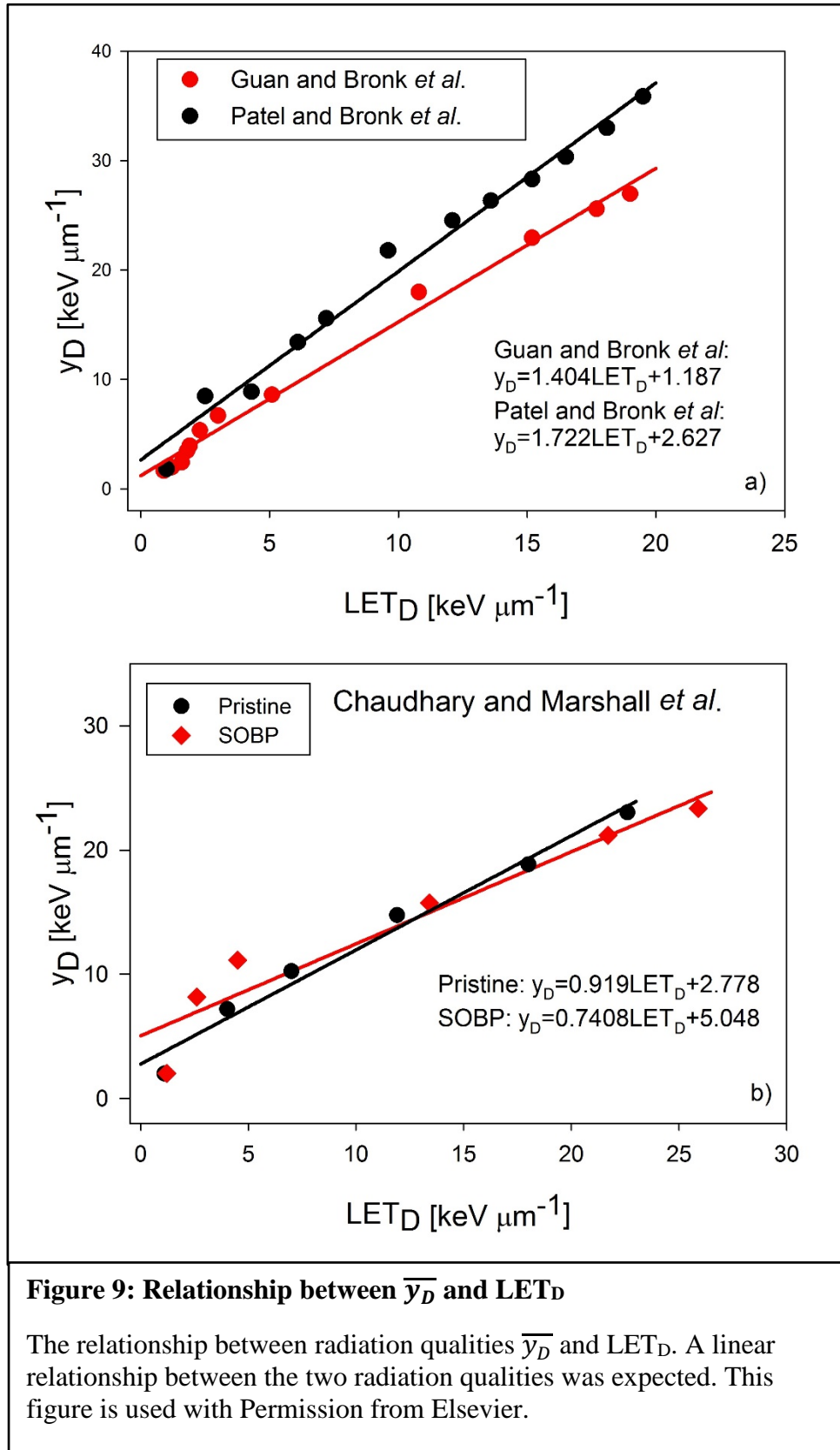


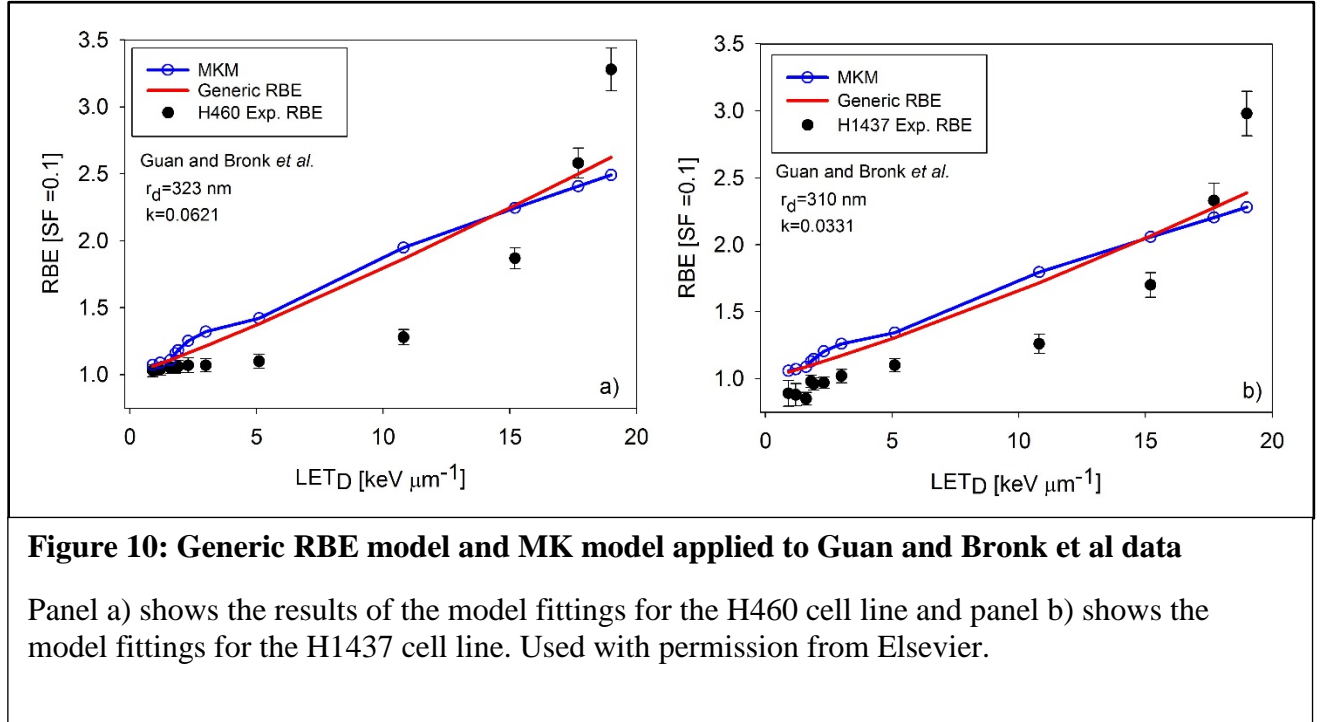
Figure 8: $\overline{y_D}$ values for monoenergetic proton beams

The $\overline{y_D}$ for each calculated $f(y)$, based on Eq. 12. The discontinuity at 100 MeV is an artifact of changing ionization models at 100 MeV. The $\overline{y_D}$ published in Ref. 37 are shown in red for comparison. This figure is used with permission from Elsevier.



3.5 Modeling RBE with the generic RBE model and the MK model

The generic RBE model from Eq. 7 was fit to the experimental data by varying k and inputting the LQ parameters listed in Table 1. By varying r_d and using the $\overline{y_D}$ calculated via Eq. 18 and Eq. 19 and using the LQ parameters from Table 1, the experimental RBE data was modeled by the MK model. The results of these fittings is presented in Figs. 10-12. In the panels of these figures are the fitted k and r_d values. Note that in Figs. 10-12, the abscissa is plotted as LET_D . This is to remain consistent with convention, but the reader should be aware that for the MK model, RBE is actually a function of $\overline{y_D}$ and not LET_D .



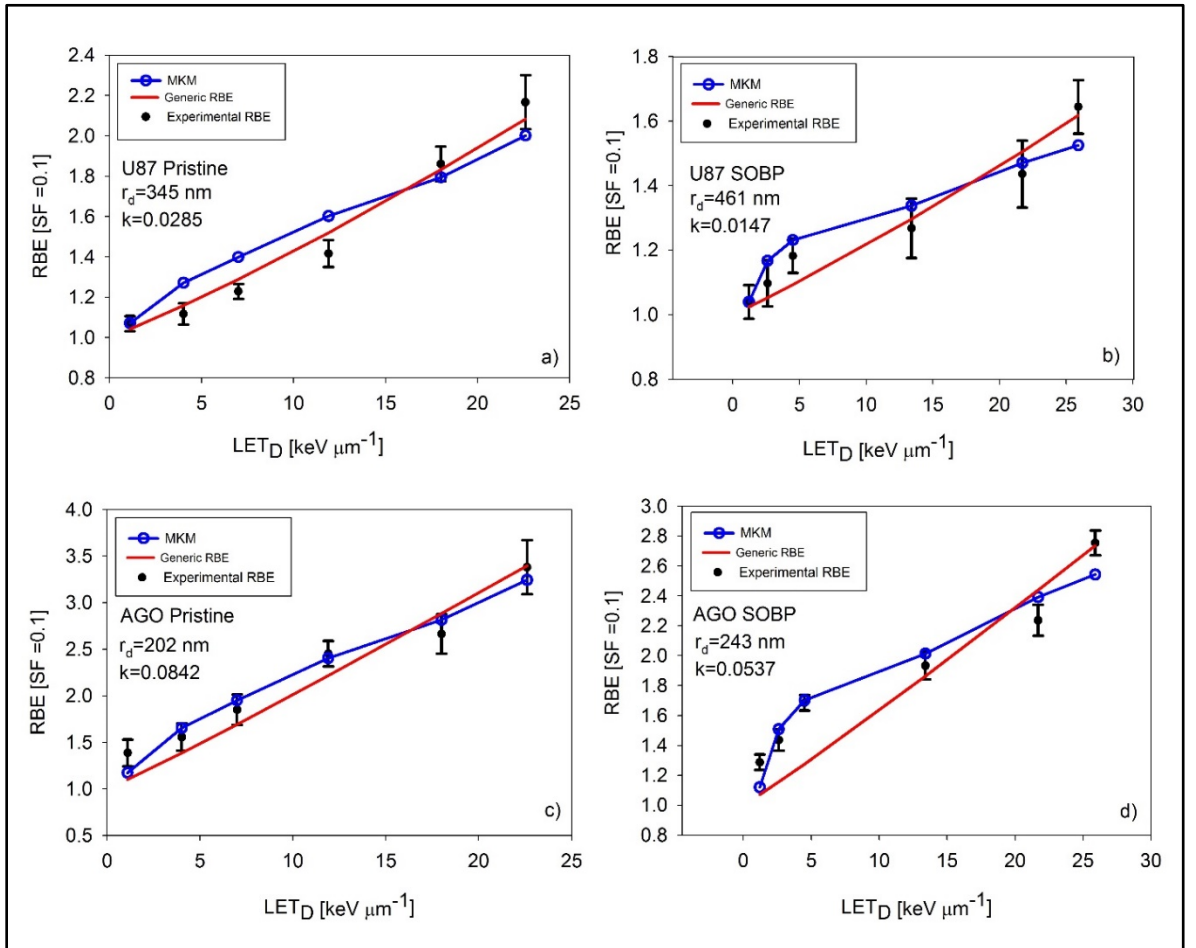
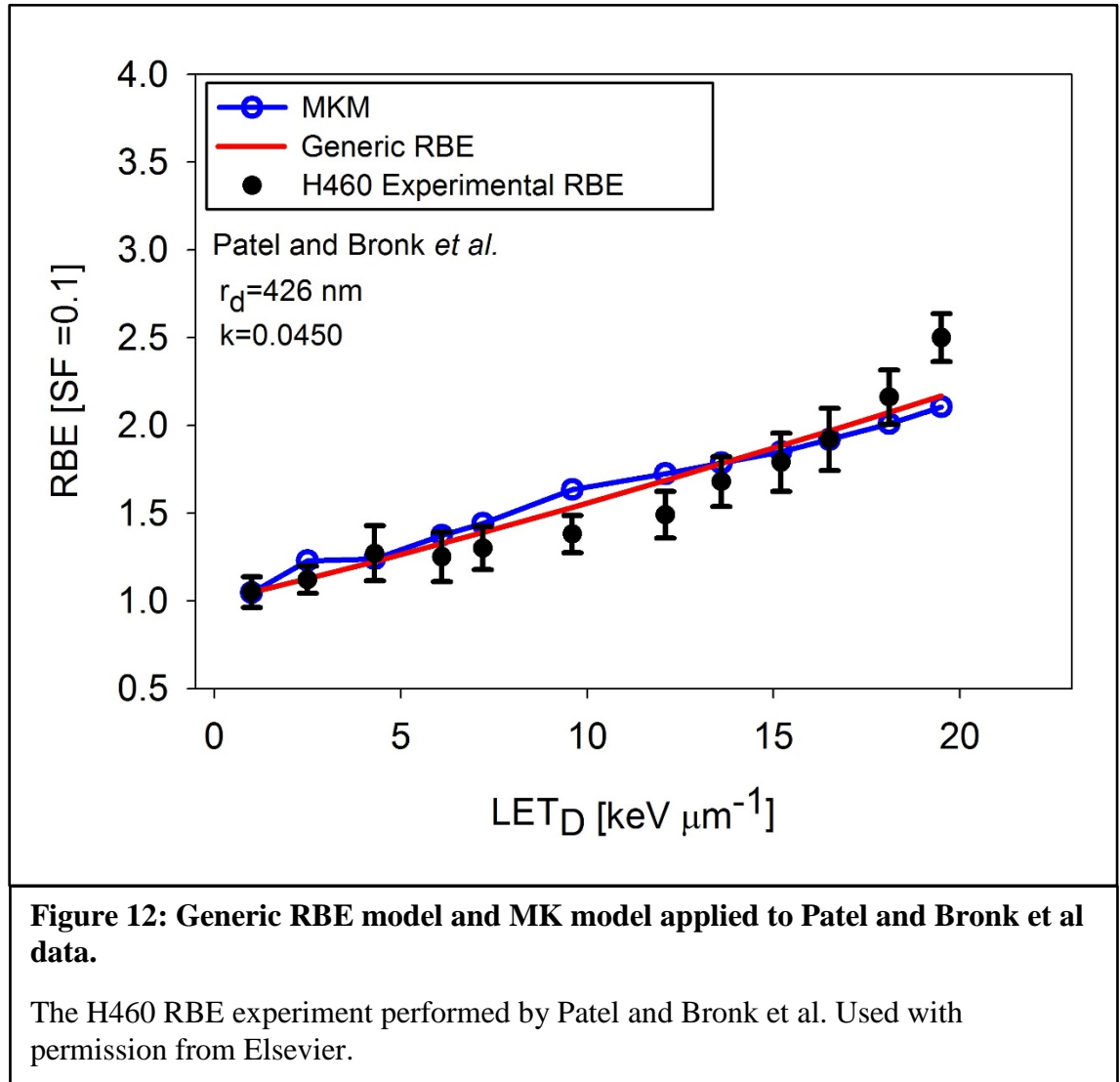


Figure 11: Generic RBE model and MK model applied to Chaudhary et al data.

Panels a) and b) show the U87 cell line experiments and model fittings in the pristine Bragg peak and spread out Bragg peak setups, respectively. Panels c) and d) show the same fittings for the same irradiation setups with the AGO1522 cell line. Used with permission from Elsevier.



3.6 AIC analysis of generic RBE model vs. the MK model

Table 9 shows the results of the AIC analysis to compare the performance of the generic RBE model and MK model. The relative likelihood from the AIC analysis is the likelihood that the worse-fitting model (in terms of a larger sum of squares) is actually the better model. MKM fit the data better in two experiments, and five experiments were fit better with the generic RBE model.

Table 9: AIC analysis of generic RBE model vs MK model

Results of the AIC analysis comparing the generic RBE model to the MK model. The RL indicates the relative likelihood that the worse-fitting model actually is superior. SS indicates the sum of squares difference between the data and the model fit.

Cell line	MKM	Generic
Guan and Bronk et al H460	$r_d = 323$ nm	$k=0.0621$
	CI=[286.7-379.3]	CI = [0.04798-0.07578]
	SS1 = 1.473	SS2 = 1.061
	RL = 0.140	-
H1437	$r_d = 310$ nm	$k=0.0330$
	CI = [274.8-368.8]	CI = [0.02511-0.04073]
	SS1 = 1.271	SS2 = 0.9396
	RL = 0.1632	-
Chaudhary et al Pristine Bragg peak, AGO1522	$r_d = 302$ nm	$k=0.08423$
	CI=[192.4-213.9]	CI=[0.07092-0.09746]
	SS2=0.1096	SS1=0.2404
	-	RL = 0.0948
Pristine Bragg peak, U87	$r_d=345$ nm	$k=0.0285$
	CI=[311.3-394.7]	CI=[0.02554-0.0313]
	SS1=0.1189	SS2=0.02386
	RL = 0.0081	-
Spread out Bragg peak, AGO1522	$r_d=243$ nm	$k=0.0537$
	CI=[227.2-262.8]	CI=[0.03957-0.06765]
	SS2=0.1086	SS1=0.3402
	-	RL = 0.0325
Spread out Bragg peak, U87	$r_d= 461$ nm	$k=0.0147$
	CI=[420.0-518.0]	CI=[0.01318-0.0194]
	SS2=0.02759	SS1=0.01614
	RL = 0.2002	-
Patel and Bronk et al H460	$r_d = 426$ nm	$k = 0.045$
	CI=[397.5-461.9]	CI=[0.03987-0.0514]
	SS1 = 0.3606	SS2 = 0.2169
	RL = 0.0474	-

3.7 matRad Optimization Results

In order to compute RBE for the MK model, $\overline{y_{D_{mix}}}$ must be calculated, which requires the $\overline{y_D}$ of each beam contributing dose at that location. Figure 13 shows an example of the $\overline{y_D}$ and integral depth doses for two beams, 88.0 MeV and 181.1 MeV, and is illustrative of the data used for MKM optimization in matRad.

Following the constraints given in Table 2 and the dose prescription of 54 Gy(RBE) to the GTV, a treatment plan using RBE=1.1 was created, known as the std_opt plan. The RBE-weighted dose (RWD) was recalculated on this treatment plan using the MK model outlined in section 2.6.1, and is called the std_opt_MKM_calc plan. Finally, a biologically optimized plan known as MKM_opt was created. Table 10 shows the GTV and CTV coverage as well as the dose to the brainstem and spinal cord and NTCP estimates for the brainstem for each plan.

Figure 14 shows the DVHs for the std_opt and std_opt_MKM_calc plans. This shows that hot spots in normal brain tissue appeared, and cold spots appeared in the brainstem when analyzing the std_opt plan with a variable RBE calculated via the MK model.

During optimization, the dose must be rapidly recalculated for each iteration. In the standard optimization algorithm (fixed RBE=1.1), each recalculation of the dose and objective function took approximately 1-3 seconds. During the MK model based optimization, each dose, RBE and objective function calculation took approximately 6-7 minutes. When running the RBE optimization algorithm, a typical optimization run would take ~6-17 hours, and require a maximum of 104 GB of memory.

Figure 15 shows the RBE distribution of the std_opt_MKM_calc plan. In most of the brainstem, $RBE < 1.1$. This is what led to the lower EUD and lower point doses to the brainstem on the std_opt_MKM_calc plan as shown in Table 10.

Hotspots appeared at the edge of the CTV and in the normal brain tissue just beyond the CTV when the variable RBE was calculated on the std_opt plan. Figure 16 shows the same CT slice with a side by side comparison of the std_opt plan and the std_opt_MKM_calc plan. The hotspot was reduced in the MKM_opt plan, and the result is shown in Fig. 17. The hotspot in the CTV was reduced, as was the RWD in the region just outside of the CTV.

Table 10: Dose to targets and OARs for IMPT plans

The doses to the optic chiasm, optic nerves and eyes were well below tolerances and are not shown.

Structure/EUD	std_opt	std_opt_MKM_calc	MKM_opt
% of GTV getting ≥ 54 Gy(RBE)	88.0	87.7	94.0
GTV EUD [Gy(RBE)]	57.0	57.8	58.3
% of CTV getting ≥ 54 Gy(RBE)	74.1	76.8	76.9
Max spinal cord dose [Gy(RBE)]	49.7	49.0	47.5
Dose to 10% of brainstem [Gy(RBE)]	54.6	52.2	54.0
Dose to 50% of brainstem [Gy(RBE)]	47.6	45.2	46.3
Dose to 0.1cc of the brainstem [Gy(RBE)]	56.2	55.8	56.0
Brainstem EUD [Gy(RBE)]	52.2	51.1	51.7
Brainstem NTCP [%]	2.9	2.0	2.4

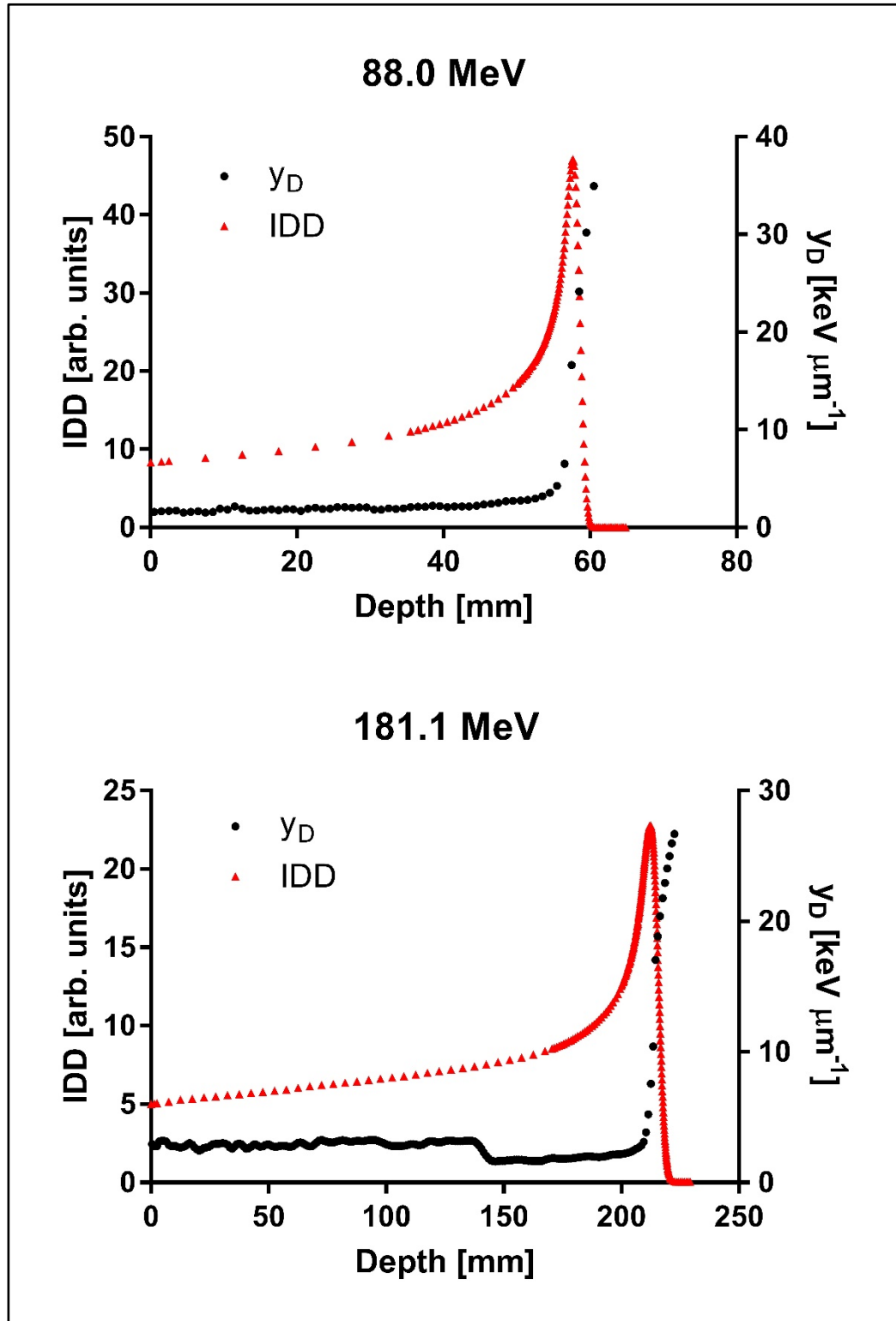


Figure 13: IDDs and $\overline{y_D}$ as a function of depth for two beams.

The $\overline{y_D}$ of the beams only increases rapidly near and beyond the Bragg peak. The bump at 140 mm is an artifact of different ionization models used by Geant4 DNA for protons at 100 MeV.

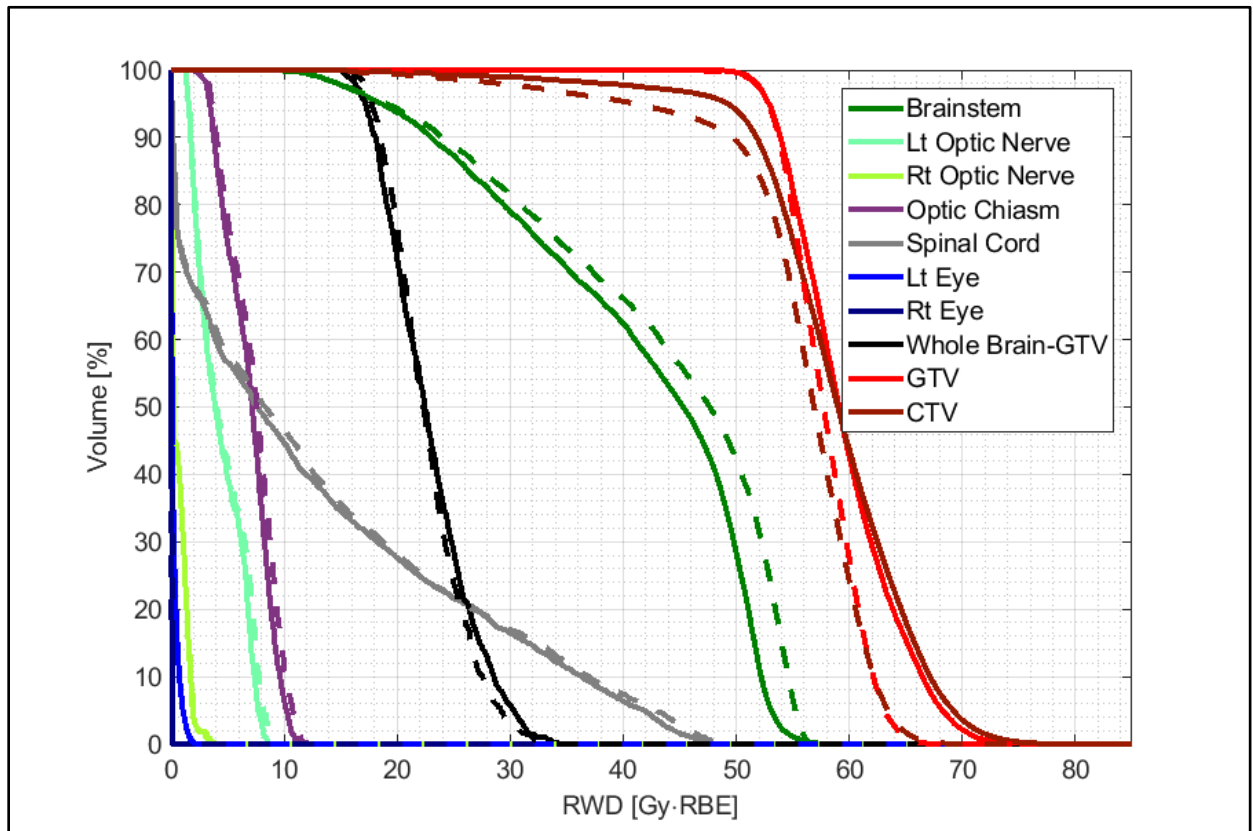


Figure 14: Dose volume histograms of the RBE-weighted doses of the std_opt and std_opt_MKM_calc plan.

The dashed lines indicate the resulting DVHs when the IMPT plan was optimized using the constant RBE=1.1 model. Solid lines are the DVHs of that same physical dose distribution with a variable RBE calculated by the MK model.

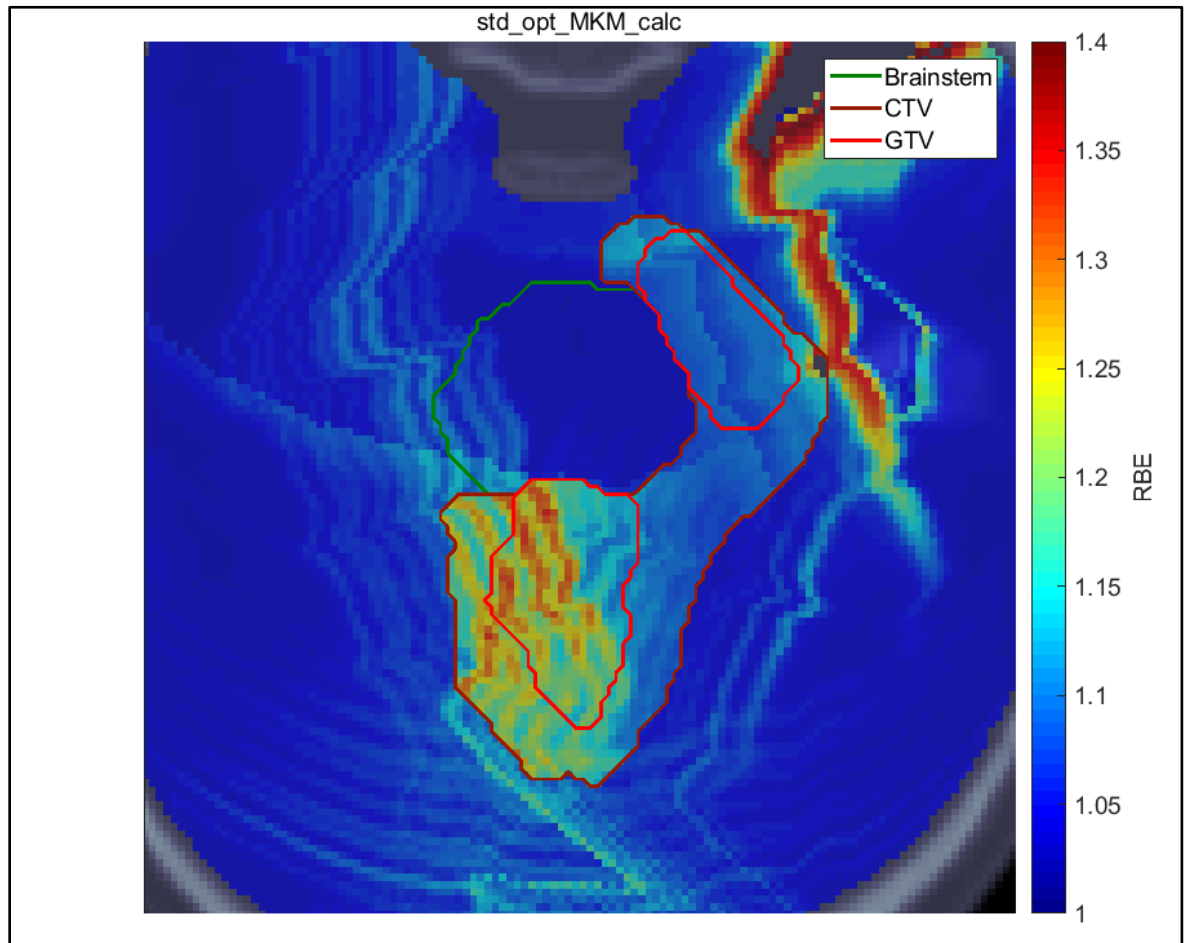
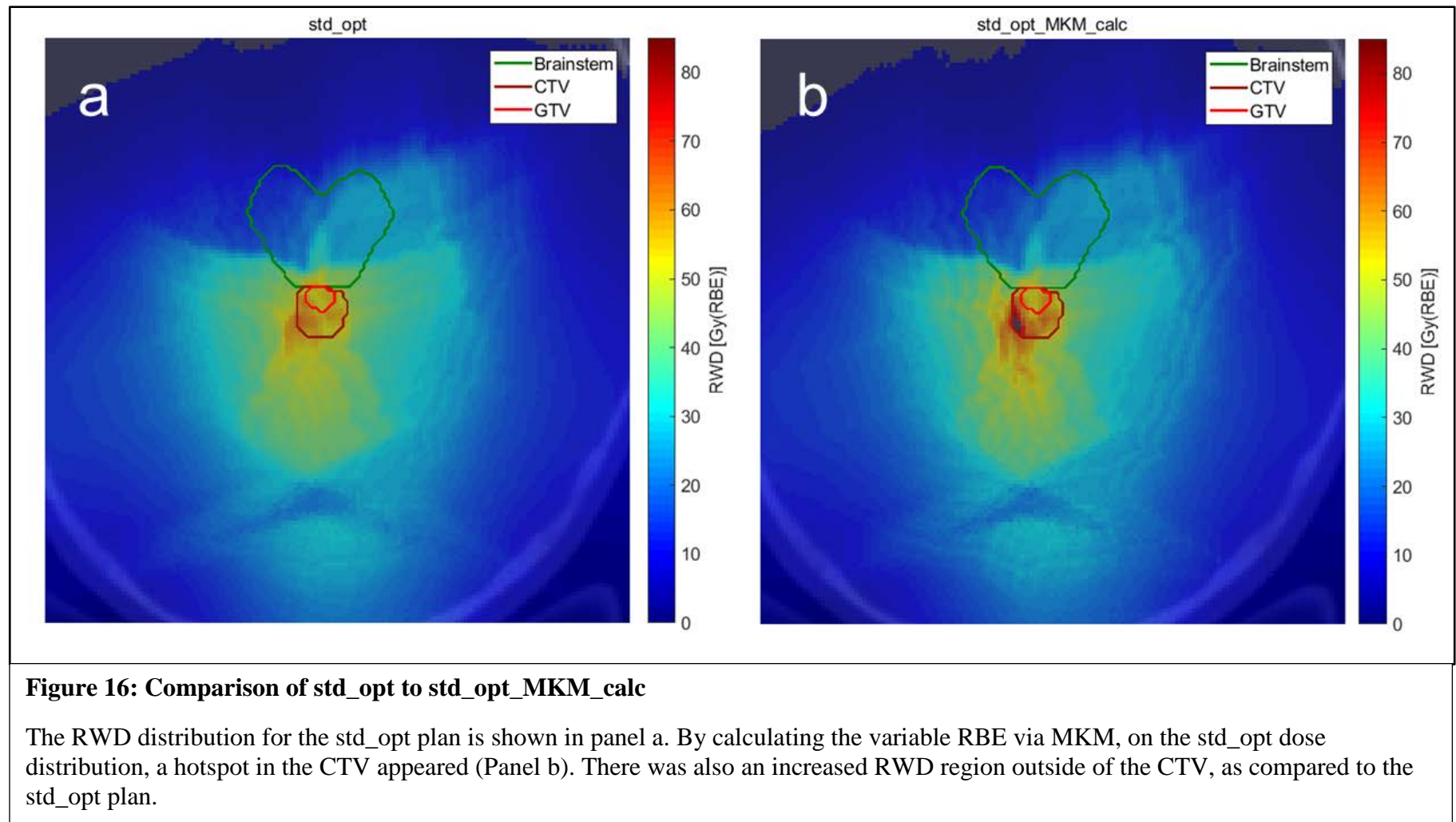


Figure 15: RBE in the brainstem, GTV and CTV as calculated by the MKM

Based on the values for α_0 , β , and r_d , the RBE in the brainstem was mostly < 1.1 . This led to decreased RWD to the brainstem when the RBE is calculated from the MK model in the std_opt_MKM_calc plan.



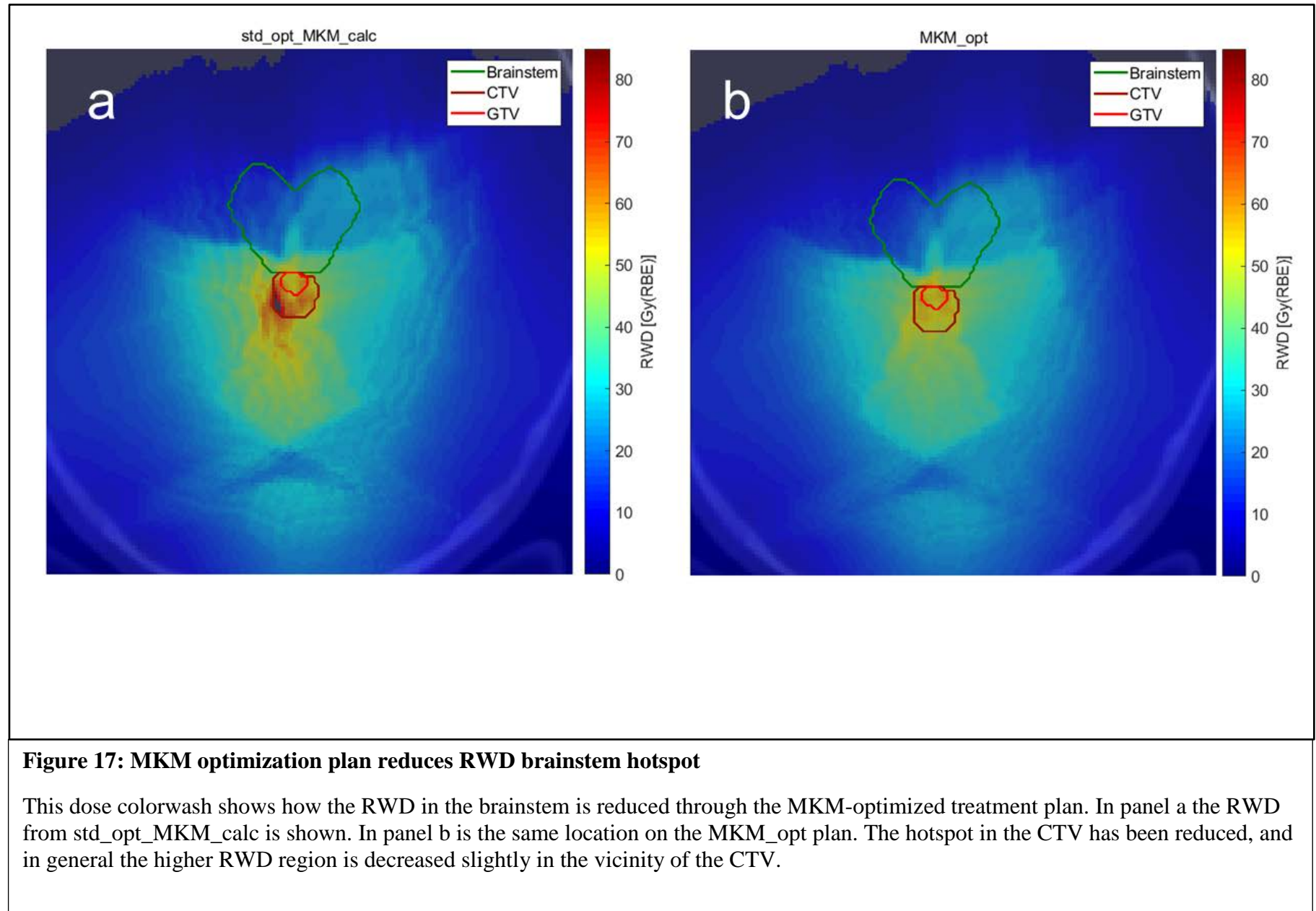


Figure 18 compares the DVHs of the std_opt_MKM_calc plan to the MKM_opt plan. This shows increased GTV coverage as well as increased RWD to the brainstem in the MKM_opt plan. In Figure 19 the $\overline{y_D}$ distribution from the std_opt plan (calculated in the std_opt_MKM_calc plan) is shown next to the $\overline{y_D}$ distribution in the MKM_opt plan. $\overline{y_D}$ was reduced in the brainstem and maintained in the GTV and CTV after RBE optimization. Figure 20 shows the physical dose difference between the MKM_opt plan and the std_opt plan. This figure demonstrates the dose modulation that occurred during the RBE optimization process, and shows that physical dose was increased into the brainstem and decreased in the GTV and CTV.

The RWD distribution in the MKM_opt plan was recalculated with the RBE=1.1 model, and the DVH of the MKM_opt plan with variable and fixed RBE (RBE=1.1) is shown in Fig. 21. Dose-volume parameters of this recalculation are shown in Table 11. To obtain the RWD of the MKM_opt plan for the RBE=1.1 model, the physical dose in the MKM_opt plan was multiplied by 1.1.

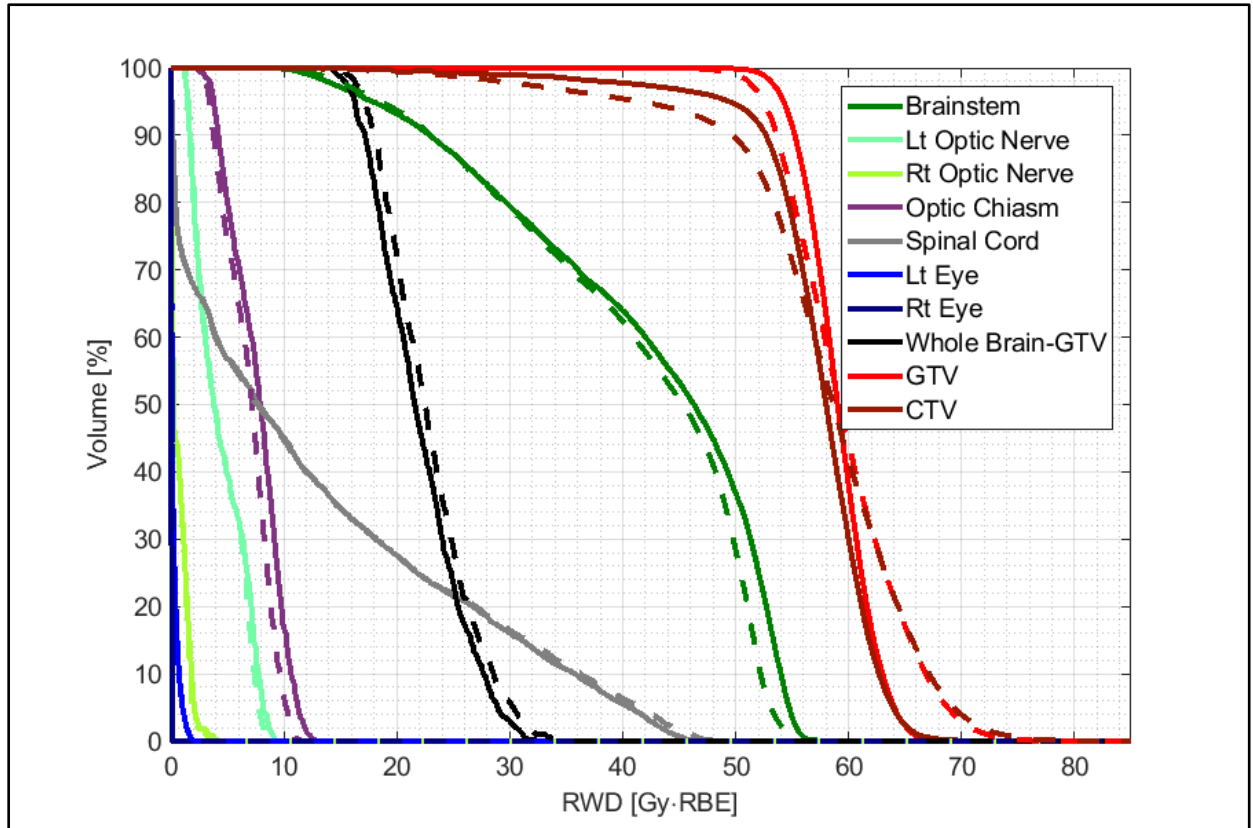


Figure 18: DVH comparison of std_opt_MKM_calc and MKM_opt

In this DVH comparison, the solid lines represent the MKM_opt plan and the dashed lines the std_opt_MKM_calc plan. Note that in this figure, the std_opt_MKM_calc plan is in dashed lines and the same plan is showed in solid lines in Fig. 14.

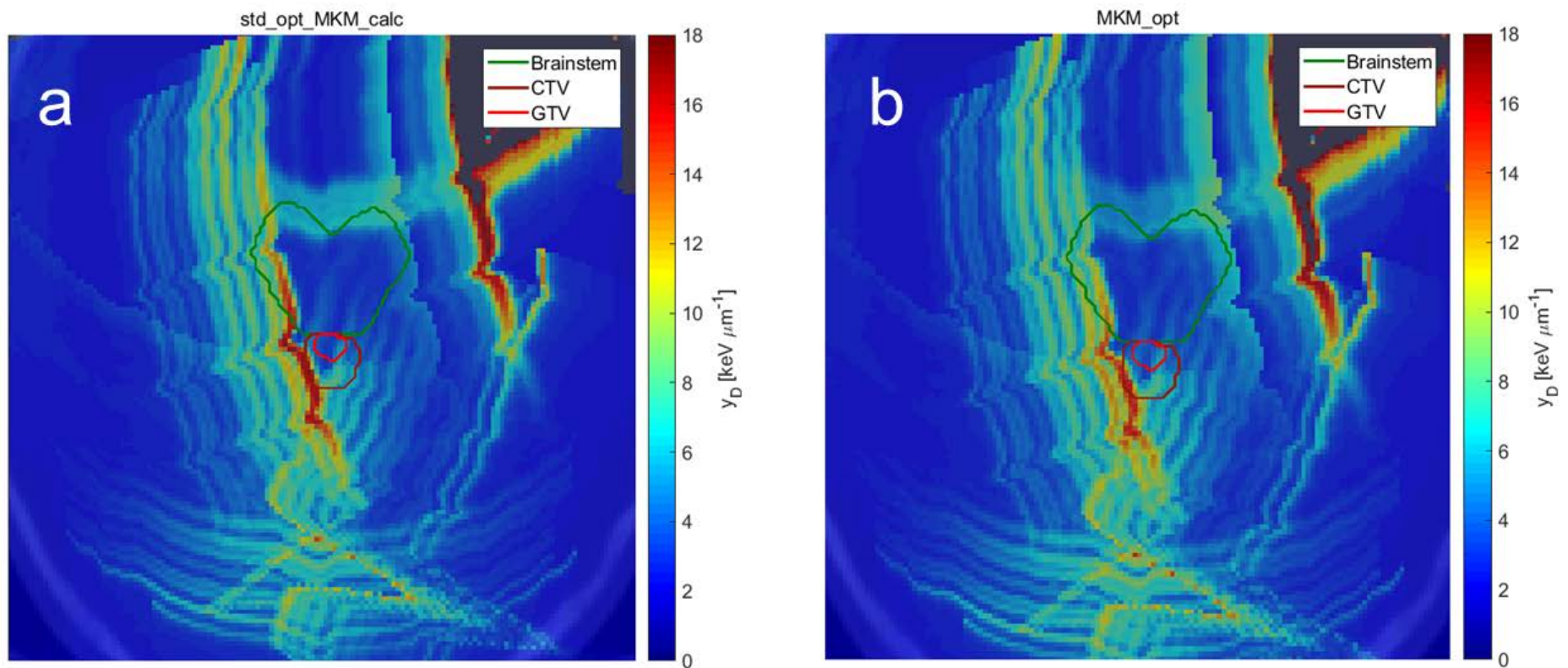


Figure 19: $\overline{y_D}$ distribution before and after MKM optimization

Panel a shows the $\overline{y_D}$ distribution in the brainstem, GTV and CTV as calculated on the std_opt plan. Panel b shows the $\overline{y_D}$ distribution after MKM optimization. The $\overline{y_D}$ in the brainstem is reduced in the MKM_opt plan, and therefore RBE in the brainstem decreases accordingly.

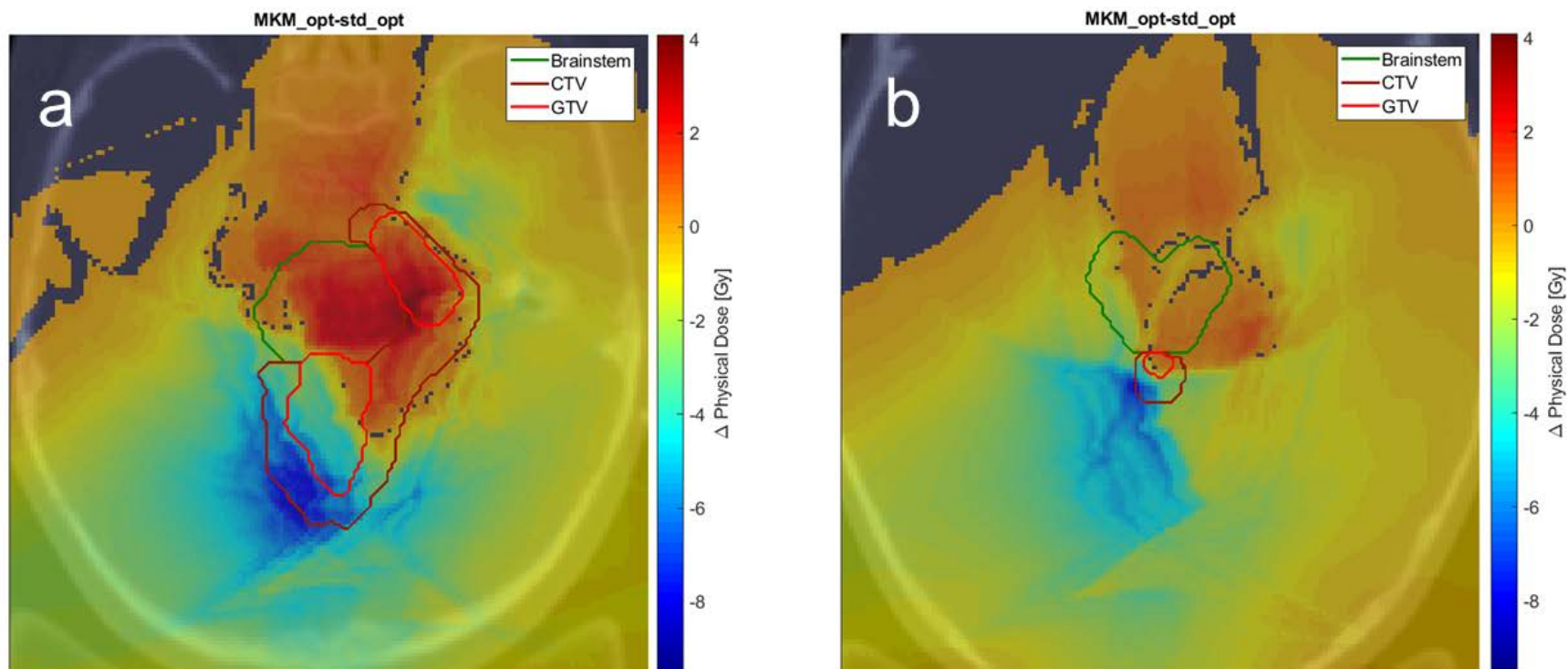


Figure 20: Difference in physical dose distributions between std_opt and MKM_opt plan

Both panels show the difference in physical dose in the two optimized plans, std_opt and MKM_opt. The slice in panel a is the same slice shown in Fig. 15, and the slice in panel b is the same slice shown in Figs. 16, 17 and 19. During the optimization process in the MKM_opt plan, the physical dose in the brainstem was increased, and the physical dose in the GTV and CTV was decreased by several Gy in some regions of those structures.

Table 11: DVH metrics for MKM optimized plan analyzed with variable RBE and RBE=1.1

Summary of the DVH metrics of the MKM_opt plan with the variable RBE, and with the MKM_opt variable RBE with the RWD recalculated using a constant RBE=1.1.

Structure/EUD	MKM_opt, Variable RBE	MKM_opt, RBE=1.1
% of GTV getting ≥ 54 Gy(RBE)	94.0	77.5
GTV EUD [Gy(RBE)]	58.3	55.9
% of CTV getting ≥ 54 Gy(RBE)	76.9	59.3
Max spinal cord dose [Gy(RBE)]	47.5	48.6
Dose to 10% of brainstem [Gy(RBE)]	54.0	56.8
Dose to 50% of brainstem [Gy(RBE)]	46.3	48.4
Dose to 0.1cc of the brainstem [Gy(RBE)]	56.0	59.1
Brainstem EUD [Gy(RBE)]	51.7	55.6
Brainstem NTCP [%]	2.4	7.4

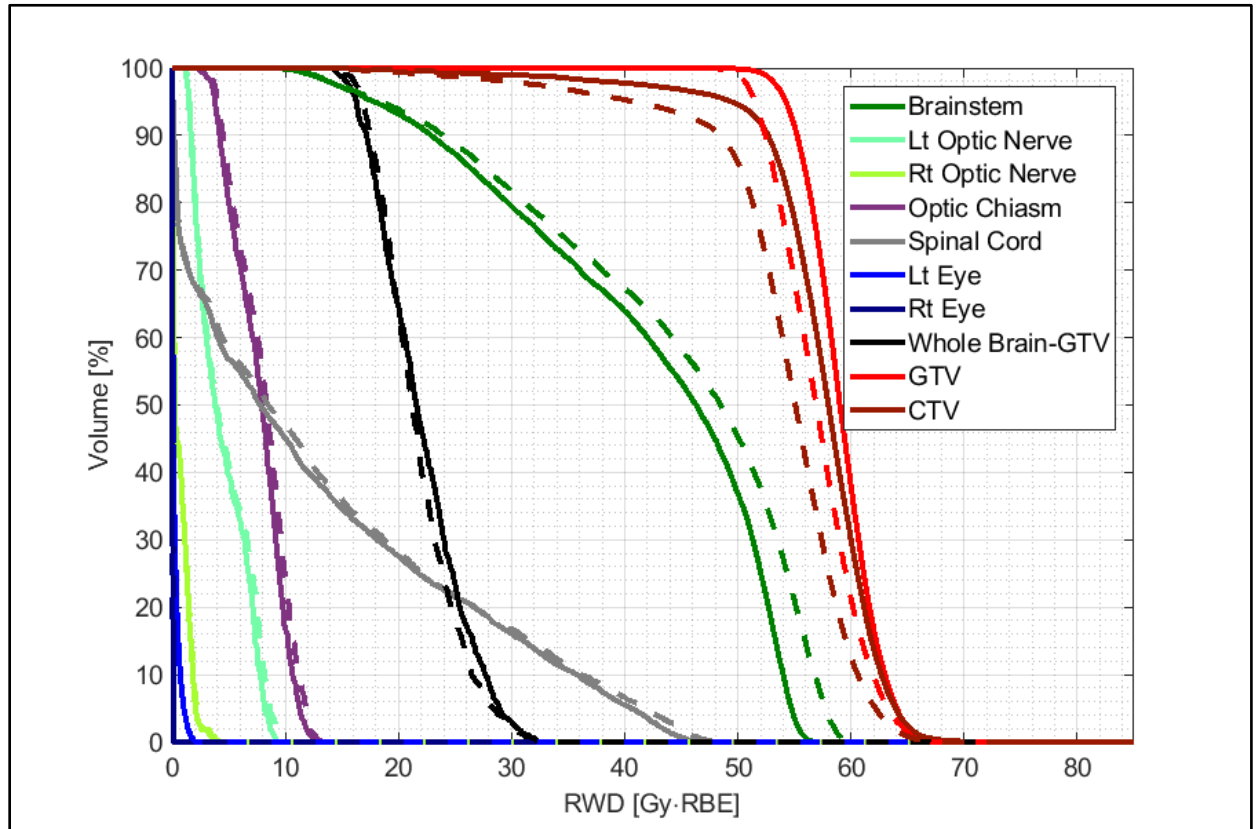


Figure 21: RWD for MKM_opt plan and MKM_opt plan recalculated with RBE = 1.1

The solid lines represent the DVH for the MKM_opt plan (same as the solid lines in Fig. 18). The dashed lines represent the DVH for the RWD of the MKM_opt plan by assuming RBE = 1.1, not the variable RBE calculated by the MK model.

Chapter 4: Discussion

4.1 Difference between phenomenological models and experimental RBE data

The phenomenological proton RBE models proposed by Wedenberg et al, McNamara et al and Carabe-Fernandez et al were applied to experimental data published by Chaudhary et al, Guan and Bronk et al and Patel and Bronk et al. These model fittings are shown in Fig. 5 and Fig 6. The percent difference between model predictions and experimental data are shown in Tables 4-8. The purpose of applying these phenomenological proton RBE models to these experiments was to determine how well the models predict RBE in the Bragg peak and distal falloff region.

For both cell lines in the Guan and Bronk et al data the phenomenological models overestimated RBE close to the Bragg peak, around 10.8 keV/ μ m, but the models underestimated RBE at higher LET_D (Fig. 5a, 5b). As remarked by McNamara et al and Guan and Bronk et al, this experimental data shows RBE as a highly nonlinear function of LET_D [18, 24]. All three of the presented models fail to account for the nonlinearity of this data set and therefore no models even follow the same shape as the data. The three models' accuracy in the H460 cell line experiments underestimated RBE by greater than 20% only at the highest two LET_D points. The H1437 data was similarly modeled by the phenomenological models, where RBE underestimation by the models was for the highest two LET_D points. The exception to this was the Carabe-Fernandez model, which overestimated RBE at the Bragg peak by 29%, and was within 8% at the 17.7 keV/ μ m LET_D point. In conclusion the phenomenological RBE models poorly model the RBE data in presented by Guan and Bronk et al.

In contrast to the striking nonlinearity of the Guan and Bronk et al data, all of the data presented by Chaudhary et al and Patel and Bronk et al show a much more linear relationship

between RBE and LET_D (Fig. 5 c-f, Fig. 6). The AGO1522 cell line in both the SOBP and pristine Bragg peak configuration was not modeled well by the phenomenological models. Each model under predicted RBE in the Bragg peak and beyond, with up to 110% difference between the Carabe-Fernandez model and experimental data. In the SOBP the AGO1522 cells (Fig. 5e) were better modeled by the phenomenological models, although in all cases the models underestimate RBE by more than 20%. AGO1522 is a normal human fibroblast cell line with a large (8.7 Gy) α/β ratio. Many malignant tumors are radioresistant and thus have smaller α/β ratios, and these results show the dangers in assuming the same radiobiological properties across a range of tissues. Ideally, different radiobiological survival parameters should be applied to different tissues in treatment planning. The U87 cell line is a radioresistant glioma cell line, and the phenomenological RBE models predict RBE much better with the U87 cells than the AGO1522 cells. In the pristine Bragg peak setup on the U87 cells (Fig. 5d), the RBE models actually overestimate RBE in the low LET_D region, but are typically within 10%. In the U87 SOBP setup (Fig. 5f) the RBE models also overestimate RBE, typically by more than 20%. Overall, phenomenological models do not model the RBE as function of LET_D well, save for the U87 pristine Bragg peak geometry.

In Fig. 10 and Table 8 the comparison of the phenomenological RBE models and RBE data is presented for the Patel and Bronk et al data. This dataset uses the same cell line, H460, as presented in Guan and Bronk et al. However the data by Patel and Bronk do not show the same degree of nonlinearity between RBE and LET_D . The reason for the differences in the two experiments is unclear, but can possibly be related to differences in cell colony counting during the clonogenic assays between the two studies, and the different Monte Carlo simulation settings between the two studies. Whatever the cause, the Patel and Bronk et al RBE as a function of LET_D was much more linear. In this data 7 out of 12 experimental measurements

were done at or beyond the Bragg peak. All three phenomenological models overestimate RBE for the points closest to the Bragg peak (9.8 and 12.3 keV/ μm). After this point RBE models underestimate RBE. However at only the highest LET_D point (20.2 keV/ μm) do the RBE models underestimate the experimental RBE by more than 20%.

4.2 Fitting the generic RBE model to data

The generic RBE model fit the experimental RBE data well, except for the very nonlinear data published by Guan and Bronk et al. In the Chaudhary et al data, the generic RBE model fits the pristine Bragg peak data better than the SOBP data, due to that data's more linear relationship between LET_D and RBE. The generic RBE model and the MK model fittings are shown in Figs. 10-12. Overall, by fitting the generic RBE model to the data, RBE is modeled well as a linear function of LET_D.

4.3 Uncertainty analysis of Geant4 DNA $f(y)$ scoring method

The uncertainty analysis of the presented Geant4 DNA scoring method to calculate $f(y)$ (Fig. 7) shows that with enough samples and enough proton tracks, a small amount of fractional error can be assured. The fractional errors for every $f(y)$ below 1×10^{-3} for protons means that when $f(y)$ functions are combined as in Eq. 19, the combined fractional error of all the individual $f(y)$ will be negligible. In Fig. 7c) the number of simulated proton tracks drops from 100 to about 70 and gradually decreases as energy increases. This is due to the change in physics models mentioned in section 4.4. The physics models used for protons with kinetic energies > 100 MeV assume that the protons interact with matter much less frequently than the models used below 100 MeV. Thus when some simulations are carried out by Geant4 DNA, the result is that the proton had no interactions in the 5 μm sided water cube, and therefore no track file was written. This was discovered during post-processing of the data. Due to the relatively low fractional error (Fig. 7a), the missing tracks were not re-simulated. The choice not to re-

simulate this data is supported by the minimal effects these higher energy protons have on the RBE calculation in the treatment planning cases, as discussed in section 4.7.

4.4 Calculating $\overline{y_D}$

The method to calculate $f_w(y)$ in Eq. 18 is a novel method to calculate $f_w(y)$ based on a fluence-weighted averaging of constituent $f(y)$. The values for $\overline{y_D}$ compare closely to those published by Nikjoo et al, Lindborg et al and Anderson et al [37, 38, 51]. The discontinuities at 100 MeV seen in Fig. 7a), c) and Fig. 8 are due to different energy models in Geant4 DNA being applied. For protons with kinetic energy < 100 MeV, the DNABornIonisationModel model is used when calculating energy losses due to ionization. For protons with energies > 100 MeV, the BetheBloch ionization model is used. The calculated $\overline{y_D}$ values published by Nikjoo et al at 100 MeV and 200 MeV are 1.8 keV/ μm and 0.5 keV/ μm , respectively [37]. The 100 MeV $\overline{y_D}$ for this work was calculated to be 2.13 keV/ μm , while the 200 MeV $\overline{y_D}$ was calculated to be 2.8 keV/ μm . A $\overline{y_D}$ value of about 3 keV/ μm at 100 MeV was published by Lindborg et al [38]. The $\overline{y_D}$ values in this work compare closely to those published by Nikjoo et al and Lindborg et al at 100 MeV, but there is a large difference at 200 MeV between this work's $\overline{y_D}$ and the $\overline{y_D}$ published by Nikjoo et al. Tsuda et al published a study of the microdosimetry of proton, helium and silicon ion beams where they compared measured $\overline{y_D}$ to those calculated by the Monte Carlo code PHITS [52]. They measured $\overline{y_D}$ of a 160 MeV proton beam to be about 2.5 keV/ μm , calculated $\overline{y_D}$ with PHITS to be about 1.98 keV/ μm . This work calculated $\overline{y_D}$ to be 2.56 keV/ μm at 160 MeV. Jing Chen published a series of microdosimetry calculations of proton beams and her $\overline{y_D}$ values at 500 keV, 2 and 5 MeV closely matched those calculated in this work [53]. However, at 100 MeV and 200 MeV, Chen calculated $\overline{y_D}$ at ~ 5 keV/ μm and 4 keV/ μm , respectively. The $\overline{y_D}$ calculated by this work is 2.1 keV/ μm at 100 MeV and 2.8 keV/ μm at 200 MeV.

Beyond the discontinuity at 100 MeV, the $\overline{y_D}$ values calculated in this work are similar to those calculated in previous works, and similar to those values measured with microdosimeters such as in Anderson et al [51]. The relationship between LET_D and $\overline{y_D}$ is shown in Fig. 9. Kellerer derived the relationship between $\overline{y_D}$ and LET_D to be $\overline{y_D} = \frac{9}{8}LET_D + \frac{3\delta_2}{2d}$, where δ_2 is the weighted energy loss per collision and d is the diameter of the domain [31]. Therefore a linear relationship between LET_D and $\overline{y_D}$ is expected.

4.5 MKM fitting of experimental RBE data

The MK model was applied to the experimental RBE data and the fitting results are shown in Figs. 10-12. Similar to the generic RBE model, the MK model fit the Guan and Bronk et al. data poorly (Fig. 10). The MK model performed well with the Patel and Bronk et al data shown in Fig. 12, as well as both AGO1522 data sets, and the U87 SOBP data from Chaudhary et al in Fig. 11. Interestingly, the MKM was able to model the fine structure from the SOBP experiments from Chaudhary et al, where RBE varies more nonlinearly with LET_D than in the pristine Bragg peak experiments. In those experiments the first three RBE points and last three RBE points seem to be linearly related, but with different slopes. The MK model was able to capture this fine structure better, most likely due to the fluence-weighted method to calculate $\overline{y_D}$ proposed in Eq. 18 and Eq. 19. This may also be evidence that $\overline{y_D}$ is a better metric for biological effect than LET_D . This result should encourage further study of the MKM for clinical adoption as all proton plans are designed using SOBPs, not pristine Bragg peaks. The best-fit r_d values are shown for each experiment in Figs. 10-12. In this work, r_d varied between 0.202 μm and 0.461 μm . Other authors have published their r_d values for various cell lines. Kase et al showed that proton RBE experiments on V79, HSG and T1 cells resulted in r_d values of 0.26

μm , $0.34 \mu\text{m}$, and $0.35 \mu\text{m}$ [54]. Mairani et al published an r_d value of $0.300 \mu\text{m}$ for proton and helium beams [55]. The r_d in this work are thus consistent with previously published values.

The data presented by Guan and Bronk et al and Patel and Bronk et al used the same cell line, H460. The Patel and Bronk et al data showed a much more linear relationship between RBE and LET_D than the Guan and Bronk et al data, however. The r_d for each experiment was very different as well. For the Guan and Bronk et al study, the best fit r_d was $0.323 \mu\text{m}$; for the Patel and Bronk et al data, the best fit r_d was $0.426 \mu\text{m}$. As Table 9 shows, both of these values fall outside of the other's 95% confidence interval. These large differences in r_d are attributed to the different Monte Carlo settings applied to simulations between the two groups, and the different methods by which surviving cell colonies were counted between the two studies. Patel and Bronk et al discuss this Monte Carlo settings issue in detail in their work [19].

4.6 AIC analysis of generic RBE model vs. MK model

Overall the AIC analysis indicated the generic RBE model fit the data best in five experiments while the MKM fit the data better in two experiments. However, neither model fit the Guan and Bronk et al data well, so the AIC analysis indicates only a weak preference for the generic RBE model over the MK model. Based on the AIC analysis there is no clear evidence that MKM models RBE better than a generic, LET_D -based model, for this dataset. Both models performed well in some experiments, and both models performed poorly in others. This work has shown that MKM can be applied to proton RBE studies and can accurately model RBE based on the $\overline{y_D}$ calculation method presented in section 2.3.3. However, the MK model does not show a clear superiority in fitting the RBE data as compared to the generic RBE model. Therefore it is concluded that there is not enough evidence to support moving away from LET_D based proton RBE models that model RBE as a linear function of LET_D . There may be some end of range RBE nonlinearities, and perhaps the assumption of a constant β is flawed, but at

present, both the generic RBE model and MKM model provide a sufficiently accurate model of RBE, even if the underlying RBE model is actually more complex.

4.7 MKM Optimization in matRad

Before proceeding with MKM optimization, a radiation oncologist evaluated the std_opt plan and gave feedback until the plan was realistic enough to begin variable RBE optimization. The DVH for the std_opt plan is shown with dashed lines in Fig. 14 and summarized in Table 10. The MK model predicted $RBE < 1.1$ throughout most of the brainstem, which led to a decrease in RWD for the brainstem in the std_opt_MKM_calc plan. The RBE in the GTV and CTV varied greatly between ~ 1.0 - 1.4 , with hot and cold RBE spots as shown in Fig. 15. Despite hot and cold RBE spots, there was very similar RWD coverage between the std_opt and std_opt_MKM_calc plans: 88.0 % of the GTV got 54 Gy(RBE) in the std_opt plan, and 87.7% of the GTV got 54 Gy(RBE) in the std_opt_MKM_calc plan. The RWD when calculating RBE with the MKM was slightly lower in the spinal cord as well. There were hot spots in the CTV and just outside the CTV in excess of 70 Gy(RBE) that are shown in Fig. 16.

That the RWD in the brainstem decreased when using the MK model is counter to previous experience with proton irradiation close to the brainstem, where evidence of $RBE > 1.1$ in the brainstem has been shown [14, 15]. This could be attributed to the choice in r_d for the brainstem during RBE optimization. r_d was set to 461 nm, but setting it to a smaller value such as 420 nm (at the lower limit of its 95% confidence interval in the U87 SOB data in Table 9) would increase the RBE, as r_d is in the denominator when calculating RBE according to Eq. 14. Based on clinical experience in irradiating the brainstem it may be more appropriate to select an r_d such that the RBE in the brainstem is ~ 1.1 , and not as low as is shown in Fig. 15.

The brain hotspot in Fig. 16 was removed during the MKM optimization process as shown in panel b of Fig. 17. Figs. 19 and 20 b show how $\overline{y_D}$ and the physical dose was

modulated to decrease the RWD hotspot. One of the most interesting results of the MKM_opt plan is the increase of physical dose to some regions of the brainstem, shown in Fig. 20 a. Due to the lower RBE (<1.1) in the brainstem, this led to a lower RWD in the brainstem in the std_opt_MKM_calc plan, which gave the optimizer freedom to increase physical dose to the brainstem in the MKM_opt plan. Table 11 shows if the physical dose from the MKM_opt plan is recalculated using the RBE=1.1 model, the RWD to 0.1cc of the brainstem increases from 56.0 to 59.1 Gy(RBE). This plan would most likely be rejected for having too high of dose to the brainstem, in addition to having significantly lower GTV and CTV coverage at 54 Gy(RBE). Without significant evidence of the superiority of using these settings for the MK model, it is unlikely to be adopted, as the recalculated RWD using the RBE=1.1 model shows a higher dose to the brainstem than is clinically acceptable. Physical dose was decreased in the hotspot region shown in Fig. 16 b and 17a, ~6-7 Gy(RBE), shown in Fig. 20 b. Fig. 20a shows the physical dose was modulated in the same slice shown in Fig. 15, and is consistent with the dose modulation seen elsewhere in the MKM_opt plan.

The MKM_opt plan resulted in better GTV coverage (94.0% getting at least 54 Gy(RBE) as compared to 87.7% in the std_opt_MKM_calc plan), despite decreasing the physical dose in some regions of the GTV. The RWD to the spinal cord also slightly decreased in the MKM_opt plan. The RWD to 0.1cc of the brainstem was increased from 55.8 Gy(RBE) to 56.0 Gy(RBE) in the MKM_opt plan as well. That the RWD increased in the brainstem is a result of increasing physical dose to the brainstem, despite a decrease of the $\overline{y_D}$ shown in Fig. 19. The increased physical dose in the brainstem is shown in Fig. 20, while the modulation of $\overline{y_D}$ between the two plans is demonstrated in Fig. 19.

A useful exercise is to analyze the physical dose distribution given by the MKM_opt plan, and recalculate the RWD using the standard RBE=1.1 model. This result is shown in Table

11. GTV coverage at 54 Gy(RBE) drops from 94.0% to 77.5%, and GTV EUD decreases from 58.3 Gy(RBE) to 55.9 Gy(RBE). The CTV coverage decreases significantly as well. The doses to the brainstem and spinal cord also increase when the MKM_opt RWD is recalculated with RBE=1.1. The DVH in Fig. 21 shows that by assuming the given MKM parameters during optimization, the resulting plan may be overdosing the brainstem and significantly reducing CTV and GTV coverage.

There are a number of issues to be aware of with the MKM optimization algorithm written into matRad in this work that need to be addressed before clinical implementation. They include:

- 1) The high RBE values seen in experiments such as in Refs. 17-19 occur only along the distal falloff region of the Bragg peak or SOBP. The rapidly rising RBE occurs within a fraction of a millimeter, in the falloff region where the dose drops dramatically across that same distance. Voxel sizes in patient planning CTs are on the order of 1 mm, so these high RBE regions are likely to be lost due to volume averaging.
- 2) In this project, the r_d for specific tissues were assumed to be the same as they are for the U87 glioma and AGO1522 fibroblast data from Ref. 17 fit for the MK model presented in this work. These values have not been clinically validated, although a similar r_d value (320 nm) was used by Inaniwa et al in their study for using MKM in the research version of their carbon ion treatment planning system [43]. Based on RBE values in the brainstem much less than 1.1, it is appropriate to reevaluate the r_d value for the brainstem. r_d should be a smaller value, perhaps around 420 nm. The result of calculating RBE in the brainstem to be mostly ~1.0 demonstrates the danger in

- translating the fitting parameters of RBE experiments directly into a TPS. All radiobiological parameters should be fully evaluated before clinical implementation.
- 3) The α_0 values used for RBE optimization marked a change from the method of using α_x laid out in Chapter 2.2-2.4. This reflects a changing concern over the course of this multi-year project that RBE experiments widely differ in the reference radiation used. For instance, in the RBE data in Ref. 17, 225 kVp x-rays are used and in Ref. 18 and 19, Cs-137 irradiation is used. In the method laid out by Frese et al in Ref. 45, α_0 has been adjusted from α_x to remove dependence on LET. Using α_0 is most consistent with the theory of the MKM, and so is used for treatment plan optimization. However the difference between α_0 and α_x in Frese et al's data are small and the difference in RBE between the two values would be negligible.
 - 4) Using a RBE defined as the dose required to reach a clonogenic cell survival fraction of 10% may not be the most accurate representation of RBE effects in vivo. Other RBE endpoints such as intestinal crypt cell regeneration, single or double strand break induction, foci of DNA repair proteins and chromosome aberrations have all been used as endpoints to model RBE [56, 57]. Overall, the alternate endpoints do not disagree with the current RBE=1.1 model, although some selected endpoints did show considerable differences. Other clinically-relevant endpoints include standardized cognitive tests, inflammation and late tissue reactions, and these are not addressed by the MK model [42].
 - 5) When creating the patient treatment plan, the exact beam geometry (beam angle and couch angle) the patient was treated with was used for IMPT optimization. These may not be the ideal angles for biologically-optimized IMPT treatments.

- 6) The method to calculate $\overline{y_{D_{mix}}}$ is very similar to using LET_D, whose drawbacks have been written about extensively [11, 12]. As proposed in this work, calculating $\overline{y_D}$ based on the proton energy spectrum may be a more accurate way to model biological effect. However with the present computational and software resources, it is not feasible to compute the proton energy spectrum in every voxel in the planning CT fast enough to be useful for optimization. GPU-based Monte Carlo systems may be fast enough for clinical implementation, however [58].
- 7) Neither of the two optimized treatment plans (std_opt or MKM_opt) were robustly optimized, either for physical dose or biologically. Including robust optimization would greatly increase the optimization time.
- 8) The IMPT plans (std_opt and MKM_opt) were probably not the best IMPT plans that could be created, due to the author's inexperience with treatment planning. However, the purpose of comparing a standard RBE=1.1 treatment plan to one with variable RBE is meant to illustrate the possible benefits of including variable RBE in optimization; namely enhanced GTV coverage and increased sparing of normal tissues. MatRad lacks many features of commercial treatment planning systems that users can utilize to fine tune the dose distribution of plans. With more time and skill, more clinically realistic plans could be created.
- 9) Despite the large discontinuity in $\overline{y_D}$ at 100 MeV (Figs. 8 and 13), this discontinuity will have a minor effect on the RBE calculation in matRad. When taking the case of predicting RBE in H460 cell line using MKM, $\alpha_x = 0.29 \text{ Gy}^{-1}$ and $\beta_x = 0.083 \text{ Gy}^{-2}$. By taking two $\overline{y_D}$ values of 0.5 keV/ μm and 2.8 keV/ μm and inputting those parameters into Eq. 14 and Eq. 15, then calculating RBE according to Eq. 20, when $\overline{y_D} = 0.5 \text{ keV}/\mu\text{m}$,

RBE = 1.013. When $\overline{y_D} = 0.5 \text{ keV}/\mu\text{m}$, RBE = 1.073. So even though $\overline{y_D}$ changes by a factor of almost six, RBE changes only by about 6%. This is a result of the MKM assumption of the insensitivity of α_p to changes at low $\overline{y_D}$ values, from Eq. 14. If the disagreement between $\overline{y_D}$ were to occur at lower energies, where $\overline{y_D}$ might be 10 vs 60 keV/ μm , the resulting RBE values would be 1.27 and 2.96, respectively. However, the discrepancy is at high energy and relatively low $\overline{y_D}$ only. Thus it can be concluded that despite the large discontinuity in $\overline{y_D}$ values as a result of different physics lists applied to Geant4 DNA, this creates a negligible change in RBE values during treatment planning in matRad.

- 10) An issue with the implementation of the biological optimization algorithm implemented into matRad is the length of time and computational resources it took to create the MKM_opt plan. Starting from the result of the std_opt_MKM_calc plan, a biologically optimized plan took ~17.2 hours to run, and required up to 104 GB of memory. If the plan has to be fine-tuned to be accepted for treatment, the plan will need to be optimized several times. However this could be somewhat mitigated by optimizing the code for speed, by modifying it to utilize GPU technology, or Matlab's multithreading capability.

Despite these drawbacks however, the RBE optimization algorithm was able to take RWD hot spots in normal tissue and modulate the physical dose and $\overline{y_D}$ to create a superior plan in MKM_opt, compared to the std_opt_MKM_calc plan, in terms of GTV coverage while still adhering to OAR dose constraints. Fine tuning the parameters for r_d , α_x and β to more clinically-realistic values may lead to a decrease in the superiority of the MKM_opt plan, but there may still be some room for improvement over plans optimized using the static RBE=1.1 model.

The AAPM TG-256 report summarizes the current state of proton RBE research [57]. One of the conclusions of the report is that based on current uncertainties in modeling RBE in normal tissues and tumors, the adoption of a clinical RBE model is premature. The RBE optimization algorithm presented here does not solve the uncertainty issues presented in TG-256, but it does mirror the conclusion of the report, that it is theoretically possible to use an RBE model in treatment plan optimization that decreases the RWD to critical structures while increasing the RWD to the GTV.

There are other methods to incorporate RBE into the optimization process that are short of a full RBE model such as the MKM. The LET distribution can be optimized to put high LET regions of the beam into the GTV and CTV, and push the low LET regions into normal tissues without significantly changing the physical dose distribution [59]. Another method is to use an LET-weighted dose model that models RBE as a function of LET [60]. Others have also proposed introducing track-end objectives into optimization, where proton track ends are terminated preferentially in the target and LET in normal tissues is decreased, without changing the dose to the target [61]. These approaches can take into account the variation in RBE with LET while avoiding the more serious uncertainties that currently plague a clinical implementation of a proton RBE model.

Chapter 5: Conclusion

5.1 Difference between phenomenological models and experimental RBE data

The hypothesis of Specific Aim One was that phenomenological RBE models will underestimate RBE in the Bragg peak and distal falloff region by 20% or more. In total, three RBE models were applied to RBE datasets and as a result, 93 predictions about RBE were made by phenomenological models. Of these 93 RBE predictions, 43 model predictions underestimate RBE by 20% or more. There is a wide range in quality of model fitting to the experimental data. For instance, the U87 cell line from Chaudhary et al is modeled well by all phenomenological models while the AGO1522 cells from the same study are poorly modeled by the models. The phenomenological models fit the experimental data of Patel and Bronk et al well, but not the data presented by Guan and Bronk et al, even though both studies utilized the same cell line. As a result of these findings, the hypothesis of Specific Aim One is accepted. In nearly half of the RBE data points, phenomenological RBE models underestimate experimental RBE by more than 20% in the Bragg peak and distal falloff region.

5.2 Comparing the MK model to a generic LET_D based RBE model

In Specific Aim Two, the hypothesis was that the proposed method to calculate $\overline{y_D}$ and input into the microdosimetric kinetic model would predict RBE at all experimental points within experimental uncertainties. As shown in Figs. 10-12 the MK model was unable to model RBE within experimental uncertainties in all experiments. Thus the hypothesis of Specific Aim Two is rejected. A goal of Specific Aim Two was to determine the optimal fitting parameters for the MKM. The optimal fitting parameters found for this work are similar to those published by other authors, and this was deemed a success.

5.3 Creating biologically-optimized treatment plans with matRad

The goal of Specific Aim Three was to implement a variable RBE optimization algorithm into matRad to create biologically optimized IMPT plans, and to determine if such an algorithm can create plans that will both increase target coverage while sparing OARs. The treatment plan example demonstrates that the RBE optimization algorithm was implemented successfully, and that biologically optimized IMPT plans can, in theory, be superior to plans optimized using the RBE=1.1 model. The advantage of these biologically optimized plans is slight, however, and a number of assumptions have been made. These assumptions have to be evaluated through clinical trials before being adopted for widespread use. However, this work has shown that in theory, biologically optimized IMPT plans can be superior to conventionally optimized plans that assume a constant RBE of 1.1. Therefore this aim is completed successfully.

5.4 Future directions

There are a number of improvements and continuations of this work. The question of whether or not RBE is a linear function of LET_D or $\overline{y_D}$ is still unanswered, and more experiments are needed to answer this question. High precision RBE measurements such as those in Refs. 17-19 and proposed by Guan et al [62] will shed light on the RBE-LET relationship. Modeling RBE with the MK model can serve as a test of the linearity of RBE as well. The work presented here could also be expanded to other cell lines, and cells that have already been studied with MKM such as V79, T1 and HSG to determine the variability of r_d in different experiments for the same cell line, as has been done with H460 in this work. The method to compute $\overline{y_D}$ can also be expanded into heavier ions such as carbon and helium, and RBE could be modeled in a similar way to this work. For heavier ions, a saturation correction would have to be included to model the overkill region.

A very promising research area is the biological optimization of treatment plans. This is a topic with considerable interest for proton therapy, but is underdeveloped. Future work could adapt this RBE calculation method into a commercial TPS and use that to do a more in-depth comparison of treatment plans using variable RBE and constant RBE of 1.1. One assumption made in the RBE calculation in matRad is the appropriateness of dose averaging of $\overline{y_D}$ from different pencil beams. The RBE calculated via the algorithm implemented into matRad should be compared to a Monte Carlo simulation of the proton energy spectra in each voxel, where $\overline{y_D}$ is calculated from Eq. 18 and Eq. 19. This would highlight differences between the two calculation methods and may provide insight as to the drawbacks of calculating RBE via the MK model and Eq. 26. A fuller assessment of the tissue-specific MKM parameters for r_d , α_0 and β also needs to be completed before this algorithm can be implemented clinically.

Chapter 6: References

1. Wilson RR. Radiological Use of Fast Protons. *Radiology*. 1946;47:487-91.
2. Paganetti H. Relative biological effectiveness (RBE) values for proton beam therapy. Variations as a function of biological endpoint, dose, and linear energy transfer. *Phys Med Biol*. 2014;419:R419-R72.
3. Sarrut D, Bardiès M, Boussion N, Freud N, Jan S, Létang J-M, Loudos G, Maigne L, Marcatili S, Mauxion T, Papadimitroulas P, Perrot Y, Pietrzyk U, Robert C, Schaart DR, Visvikis D, Buvat I. A review of the use and potential of the GATE Monte Carlo simulation code for radiation therapy and dosimetry applications. *Med Phys*. 2014;41:064301.
4. Jan S, Benoit D, Becheva E, Carlier T, Cassol F, Descourt P, Frisson T, Grevillot L, Guigues L, Maigne L, Morel C, Perrot Y, Rehfeld N, Sarrut D, Schaart DR, Stute S, Pietrzyk U, Visvikis D, Zahra N, Buvat I. GATE V6: a major enhancement of the GATE simulation platform enabling modelling of CT and radiotherapy. *Physics in Medicine & Biology*. 2011;56:881.
5. Battistoni G, Bauer J, Boehlen TT, Cerutti F, Chin MPW, Dos Santos Augusto R, Ferrari A, Ortega PG, Kozłowska W, Magro G, Mairani A, Parodi K, Sala PR, Schoofs P, Tessonnier T, Vlachoudis V. The FLUKA Code: An Accurate Simulation Tool for Particle Therapy. *Frontiers in oncology*. 2016;6:116-.
6. Agostinelli S, Allison J, Amako K, Apostolakis J, Araujo H, Arce P, Asai M, Axen D, Banerjee S, Barrand G, Behner F, Bellagamba L, Boudreau J, Broglia L, Brunengo A, Burkhardt H, Chauvie S, Chuma J, Chytrcek R, Cooperman G, Cosmo G, Degtyarenko P, Dell'Acqua A, Depaola G, Dietrich D, Enami R, Feliciello A, Ferguson C, Fesefeldt H, Folger G, Foppiano F, Forti A, Garelli S, Giani S, Giannitrapani R, Gibin D, Gómez

- Cadenas JJ, González I, Gracia Abril G, Greeniaus G, Greiner W, Grichine V, Grossheim A, Guatelli S, Gumplinger P, Hamatsu R, Hashimoto K, Hasui H, Heikkinen A, Howard A, Ivanchenko V, Johnson A, Jones FW, Kallenbach J, Kanaya N, Kawabata M, Kawabata Y, Kawaguti M, Kelner S, Kent P, Kimura A, Kodama T, Kokoulin R, Kossov M, Kurashige H, Lamanna E, Lampén T, Lara V, Lefebure V, Lei F, Liendl M, Lockman W, Longo F, Magni S, Maire M, Medernach E, Minamimoto K, Mora de Freitas P, Morita Y, Murakami K, Nagamatu M, Nartallo R, Nieminen P, Nishimura T, Ohtsubo K, Okamura M, O'Neale S, Oohata Y, Paech K, Perl J, Pfeiffer A, Pia MG, Ranjard F, Rybin A, Sadilov S, Di Salvo E, Santin G, Sasaki T, Savvas N, Sawada Y, Scherer S, Sei S, Sirotenko V, Smith D, Starkov N, Stoecker H, Sulkimo J, Takahata M, Tanaka S, Tcherniaev E, Safai Tehrani E, Tropeano M, Truscott P, Uno H, Urban L, Urban P, Verderi M, Walkden A, Wander W, Weber H, Wellisch JP, Wenaus T, Williams DC, Wright D, Yamada T, Yoshida H, Zschiesche D. Geant4—a simulation toolkit. *Nucl Instrum Methods Phys Res A*. 2003;506:250-303.
7. Perl J, Shin J, Schümann J, Faddegon B, Paganetti H. TOPAS: An innovative proton Monte Carlo platform for research and clinical applications. *Med Phys*. 2012;39:6818.
 8. Hirayama S, Matsuura T, Ueda H, Fujii Y, Fujii T, Takao S, Miyamoto N, Shimizu S, Fujimoto R, Umegaki K, Shirato H. An analytical dose-averaged LET calculation algorithm considering the off-axis LET enhancement by secondary protons for spot-scanning proton therapy. *Med Phys*. 2018;45:3404-16.
 9. Sanchez-Parcerisa D, Cortes-Giraldo MA, Dolney D, Kondrla M, Fager M, Carabe A. Analytical calculation of proton linear energy transfer in voxelized geometries including secondary protons. *Phys Med Biol*. 2016;61:1705-21.

10. Sørensen BS, Overgaard J, Bassler N. In vitro RBE-LET dependence for multiple particle types. *Acta Oncol.* 2011;50:757-62.
11. Grün R, Friedrich T, Traneus E, Scholz M. Is the dose-averaged LET a reliable predictor for the relative biological effectiveness? *Med Phys.* 2019;46:1064-74.
12. Mohan R, Peeler CR, Guan F, Bronk L, Cao W, Grosshans DR. Radiobiological issues in proton therapy. *Acta Oncol.* 2017:1-7.
13. Peeler CR, Mirkovic D, Titt U, Blanchard P, Gunther JR, Mahajan A, Mohan R, Grosshans DR. Clinical evidence of variable proton biological effectiveness in pediatric patients treated for ependymoma. *Radiother Oncol.* 2016;121:395-401.
14. Mohan R, Held KD, Story MD, Grosshans D, Capala J. Proceedings of the National Cancer Institute Workshop on Charged Particle Radiobiology. *International Journal of Radiation Oncology*Biology*Physics.* 2018;100:816-31.
15. Haas-Kogan D, Indelicato D, Paganetti H, Esiashvili N, Mahajan A, Yock T, Flampouri S, MacDonald S, Fouladi M, Stephen K, Kalapurakal J, Terezakis S, Kooy H, Grosshans D, Makrigiorgos M, Mishra K, Poussaint TY, Cohen K, Fitzgerald T, Gondi V, Liu A, Michalski J, Mirkovic D, Mohan R, Perkins S, Wong K, Vikram B, Buchsbaum J, Kun L. National Cancer Institute Workshop on Proton Therapy for Children: Considerations Regarding Brainstem Injury. *International Journal of Radiation Oncology*Biology*Physics.* 2018;101:152-68.
16. Underwood TSA, Grassberger C, Bass R, MacDonald SM, Meyersohn NM, Yeap BY, Jimenez RB, Paganetti H. Asymptomatic Late-phase Radiographic Changes Among Chest-Wall Patients Are Associated With a Proton RBE Exceeding 1.1. *International Journal of Radiation Oncology*Biology*Physics.* 2018;101:809-19.

17. Chaudhary P, Marshall TI, Perozziello FM, Manti L, Currell FJ, Hanton F, McMahon SJ, Kavanagh JN, Cirrone GA, Romano F, Prise KM, Schettino G. Relative biological effectiveness variation along monoenergetic and modulated Bragg peaks of a 62-MeV therapeutic proton beam: a preclinical assessment. *Int J Radiat Oncol Biol Phys*. 2014;90:27-35.
18. Guan F, Bronk L, Titt U, Lin SH, Mirkovic D, Kerr MD, Zhu XR, Dinh J, Sobieski M, Stephan C, Peeler CR, Taleei R, Mohan R, Grosshans DR. Spatial mapping of the biologic effectiveness of scanned particle beams: towards biologically optimized particle therapy. *Sci Rep*. 2015;5:9850.
19. Patel D, Bronk L, Guan F, Peeler CR, Brons S, Dokic I, Abdollahi A, Rittmüller C, Jäkel O, Grosshans D, Mohan R, Titt U. Optimization of Monte Carlo particle transport parameters and validation of a novel high throughput experimental setup to measure the biological effects of particle beams. *Med Phys*. 2017;44:6061-73.
20. Rørvik E, Fjæra LF, Dahle TJ, Dale JE, Engeseth GM, Stokkevåg CH, Thörnqvist S, Ytre-Hauge KS. Exploration and application of phenomenological RBE models for proton therapy. *Physics in Medicine & Biology*. 2018;63:185013.
21. Wedenberg M, Lind BK, Hardemark B. A model for the relative biological effectiveness of protons: the tissue specific parameter alpha/beta of photons is a predictor for the sensitivity to LET changes. *Acta Oncol*. 2013;52:580-8.
22. Carabe-Fernandez A, Dale RG, Jones B. The incorporation of the concept of minimum RBE (RBE_{min}) into the linear-quadratic model and the potential for improved radiobiological analysis of high-LET treatments. *Int J of Radiat Biol*. 2007;83:27-39.

23. Carabe A, Moteabbed M, Depauw N, Schuemann J, Paganetti H. Range uncertainty in proton therapy due to variable biological effectiveness. *Phys Med Biol.* 2012;57:1159-72.
24. McNamara AL, Schuemann J, Paganetti H. A phenomenological relative biological effectiveness (RBE) model for proton therapy based on all published in vitro cell survival data. *Phys Med Biol.* 2015;60:8399-416.
25. Jones B. Towards Achieving the Full Clinical Potential of Proton Therapy by Inclusion of LET and RBE Models. *Cancers.* 2015;7:460-80.
26. Hawkins RB. A microdosimetric-kinetic theory of the dependence of the RBE for cell death on LET. *Med Phys.* 1998;25:1157-70.
27. Hawkins RB. A Microdosimetric-Kinetic Model for the Effect of Non-Poisson Distribution of Lethal Lesions on the Variation of RBE with LET. *Journal of radiation research.* 2003;160:61-9.
28. Kellerer AM, Rossi HH. The theory of dual radiation action. *Curr. Top. Radiat. Res. Q.* 1972;8:85-158.
29. Zaider M, Rossi HH. The Synergistic Effects of Different Radiations. *Radiation Research.* 1980;83:732-9.
30. ICRU. ICRU Report 36: Microdosimetry, 1983. Accessed at:
31. Kellerer AM, editor. Fundamentals of Microdosimetry. New York: Academic Press; 1985.
32. Kase Y, Kanai T, Matsumoto Y, Furusawa Y, Okamoto H, Asaba T, Sakama M, Shinoda H. Microdosimetric measurements and estimation of human cell survival for heavy-ion beams. *Radiat Res.* 2006;166:629-38.

33. Incerti S, Baldacchino G, Bernal M, Capra R, Champion C, Francis Z, GuèYe P, Mantero A, Mascialino B, Moretto P, Nieminen P, Villagrasa C, Zacharatou C. THE GEANT4-DNA PROJECT. *International Journal of Modeling, Simulation, and Scientific Computing*. 2010;01:157-78.
34. Incerti S, Ivanchenko A, Karamitros M, Mantero A, Moretto P, Tran HN, Mascialino B, Champion C, Ivanchenko VN, Bernal MA, Francis Z, Villagrasa C, Baldacchino G, Guèye P, Capra R, Nieminen P, Zacharatou C. Comparison of GEANT4 very low energy cross section models with experimental data in water. *Med Phys*. 2010;37:4692-708.
35. Bernal MA, Bordage MC, Brown JMC, Davídková M, Delage E, El Bitar Z, Enger SA, Francis Z, Guatelli S, Ivanchenko VN, Karamitros M, Kyriakou I, Maigne L, Meylan S, Murakami K, Okada S, Payno H, Perrot Y, Petrovic I, Pham QT, Ristic-Fira A, Sasaki T, Štěpán V, Tran HN, Villagrasa C, Incerti S. Track structure modeling in liquid water: A review of the Geant4-DNA very low energy extension of the Geant4 Monte Carlo simulation toolkit. *Physica Medica*. 2015;31:861-74.
36. Incerti S, Kyriakou I, Bernal MA, Bordage MC, Francis Z, Guatelli S, Ivanchenko V, Karamitros M, Lampe N, Lee SB, Meylan S, Min CH, Shin WG, Nieminen P, Sakata D, Tang N, Villagrasa C, Tran HN, Brown JMC. Geant4-DNA example applications for track structure simulations in liquid water: A report from the Geant4-DNA Project. *Med Phys*. 2018;45:e722-e39.
37. Nikjoo H, Emfietzoglou D, Liamsuwan T, Taleei R, Liljequist D, Uehara S. Radiation track, DNA damage and response-a review. *Rep Prog Phys*. 2016;79:116601.

38. Lindborg L, Hultqvist M, Å Carlsson T, Nikjoo H. Lineal energy and radiation quality in radiation therapy: model calculations and comparison with experiment. *Physics in Medicine & Biology*. 2013;58:3089.
39. Wieser H-P, Cisternas E, Wahl N, Ulrich S, Stadler A, Mescher H, Mueller L-R, Klinge T, Gabrys H, Burigo L, Mariani A, Ecker S, Ackermann B, Ellerbrock M, Parodi K, Jaekel O, Bangert M. Development of the open-source dose calculation and optimization toolkit matRad. *Med Phys*. 2017;44:2556-68.
40. Elsässer T, Weyrather WK, Friedrich T, Durante M, Iancu G, Krämer M, Kragl G, Brons S, Winter M, Weber K-J, Scholz M. Quantification of the Relative Biological Effectiveness for Ion Beam Radiotherapy: Direct Experimental Comparison of Proton and Carbon Ion Beams and a Novel Approach for Treatment Planning. *International Journal of Radiation Oncology*Biophysics*. 2010;78:1177-83.
41. Gillin MT, Sahoo N, Bues M, Ciangaru G, Sawakuchi G, Poenisch F, Arjomandy B, Martin C, Titt U, Suzuki K, Smith AR, Zhu XR. Commissioning of the discrete spot scanning proton beam delivery system at the University of Texas M.D. Anderson Cancer Center, Proton Therapy Center, Houston. *Med Phys*. 2010;37:154-63.
42. Lühr A, von Neubeck C, Pawelke J, Seidlitz A, Peitzsch C, Bentzen SM, Bortfeld T, Debus J, Deutsch E, Langendijk JA, Loeffler JS, Mohan R, Scholz M, Sørensen BS, Weber DC, Baumann M, Krause M. “Radiobiology of Proton Therapy”: Results of an international expert workshop. *Radiotherapy and Oncology*. 2018;128:56-67.
43. Inaniwa T, Furukawa T, Kase Y, Matsufuji N, Toshito T, Matsumoto Y, Furusawa Y, Noda K. Treatment planning for a scanned carbon beam with a modified microdosimetric kinetic model. *Phys Med Biol*. 2010;55:6721-37.

44. Titt U, Liu A, Mirkovic D. SU-E-T-523: Runtime Optimization for the Automatic Monte Carlo Dose Computation System MC2. *Med Phys.* 2013;40:326-.
45. Frese MC, Wilkens JJ, Huber PE, Jensen AD, Oelfke U, Taheri-Kadkhoda Z. Application of Constant vs. Variable Relative Biological Effectiveness in Treatment Planning of Intensity-Modulated Proton Therapy. *International Journal of Radiation Oncology • Biology • Physics.* 2011;79:80-8.
46. Ågren Cronqvist A-K. Quantification of the response of heterogeneous tumours and organized normal tissues to fractionated radiotherapy. PhD Dissertation. Stockholm: Stockholm University; 1995.
47. Niemierko A. A generalized concept of equivalent uniform dose (EUD). . *Med Phys.* 1999;26.
48. Niemierko A. A unified model of tissue response to radiation. 41st Annual AAPM Meeting. Nashville, TN: Medical Physics; 1999. p. p. 1100.
49. Gay HA, Niemierko A. A free program for calculating EUD-based NTCP and TCP in external beam radiotherapy. *Physica Medica.* 2007;23:115-25.
50. Newpower M, Patel D, Bronk L, Guan F, Chaudhary P, McMahon SJ, Prise KM, Schettino G, Grosshans DR, Mohan R. Using the Proton Energy Spectrum and Microdosimetry to Model Proton Relative Biological Effectiveness. *International Journal of Radiation Oncology*Biology*Physics.* 2019;104:316-24.
51. Anderson SE, Furutani KM, Tran LT, Chartier L, Petasecca M, Lerch M, Prokopovich DA, Reinhard M, Perevertaylo VL, Rosenfeld AB, Herman MG, Beltran C. Microdosimetric measurements of a clinical proton beam with micrometer-sized solid-state detector. *Med Phys.* 2017;44:6029-37.

52. Tsuda S, Sato T, Takahashi F, Satoh D, Sasaki S, Namito Y, Iwase H, Ban S, Takada M. Systematic Measurement of Lineal Energy Distributions for Proton, He and Si Ion Beams Over a Wide Energy Range Using a Wall-less Tissue Equivalent Proportional Counter. *Journal of radiation research*. 2012;53:264-71.
53. Chen J. Microdosimetric characteristics of proton beams from 50 keV to 200 MeV. *Radiation Protection Dosimetry*. 2010;143:436-9.
54. Kase Y, Kanai T, Matsufuji N, Furusawa Y, Elsasser T, Scholz M. Biophysical calculation of cell survival probabilities using amorphous track structure models for heavy-ion irradiation. *Phys Med Biol*. 2008;53:37-59.
55. Mairani A, Magro G, Tessonier T, Bohlen TT, Molinelli S, Ferrari A, Parodi K, Debus J, Haberer T. Optimizing the modified microdosimetric kinetic model input parameters for proton and (4)He ion beam therapy application. *Phys Med Biol*. 2017;62:N244-N56.
56. Cuaron JJ, Chang C, Lovelock M, Higginson DS, Mah D, Cahlon O, Powell S. Exponential Increase in Relative Biological Effectiveness Along Distal Edge of a Proton Bragg Peak as Measured by Deoxyribonucleic Acid Double-Strand Breaks. *Int J Radiat Oncol Biol Phys*. 2016;95:62-9.
57. Paganetti H, Blakely E, Carabe-Fernandez A, Carlson DJ, Das IJ, Dong L, Grosshans D, Held KD, Mohan R, Moiseenko V, Niemierko A, Stewart RD, Willers H. Report of the AAPM TG-256 on the relative biological effectiveness of proton beams in radiation therapy. *Med Phys*. 2019;46:e53-e78.
58. Wan Chan Tseung HS, Ma J, Kreofsky CR, Ma DJ, Beltran C. Clinically Applicable Monte Carlo-based Biological Dose Optimization for the Treatment of Head and Neck Cancers With Spot-Scanning Proton Therapy. *International Journal of Radiation Oncology*Biophysics*. 2016;95:1535-43.

59. Cao W, Khabazian A, Yepes PP, Lim G, Poenisch F, Grosshans DR, Mohan R. Linear energy transfer incorporated intensity modulated proton therapy optimization. *Physics in Medicine & Biology*. 2017;63:015013.
60. McMahon SJ, Paganetti H, Prise KM. LET-weighted doses effectively reduce biological variability in proton radiotherapy planning. *Physics in Medicine & Biology*. 2018;63:225009.
61. Traneus E, Ödén J. Introducing Proton Track-End Objectives in Intensity Modulated Proton Therapy Optimization to Reduce Linear Energy Transfer and Relative Biological Effectiveness in Critical Structures. *International Journal of Radiation Oncology • Biology • Physics*. 2019;103:747-57.
62. Guan F, Geng C, Ma D, Bronk L, Kerr M, Li Y, Gates D, Kroger B, Sahoo N, Titt U, Grosshans D, Mohan R. RBE Model-Based Biological Dose Optimization for Proton Radiobiology Studies. *International Journal of Particle Therapy*. 2018;5:160-71.

Vita

Mark Andrew Newpower was born in Grand Forks, North Dakota, the son of Scott and Mary Newpower. After completing high school at Skyview High School in Billings, Montana in 2008, he matriculated to Embry-Riddle Aeronautical University in Daytona Beach, Florida. He received his Bachelor of Science (cum laude) with a major in Space Physics and minors in Applied Mathematics, Astronomy and International Relations in August, 2013. He then matriculated to the University of Oklahoma Health Sciences Center in August, 2013 and received his Master of Science degree in Radiological Science in August 2015. In August of 2015 he entered the Medical Physics Doctor of Philosophy program at the University of Texas MD Anderson Cancer Center UTHealth Graduate School of Biomedical Sciences.

Permanent address:

227 Skyport Way
Seeley Lake, MT 59868